

1 **Carbon cycle feedbacks in an idealized and a scenario simulation of negative emissions in CMIP6**
2 **Earth system models**

3
4 Ali Asaadi¹, Jörg Schwinger¹, Hanna Lee^{1,2}, Jerry Tjiputra¹, Vivek Arora³, Roland Séférian⁴, Spencer
5 Liddicoat⁵, Tomohiro Hajima⁶, Yeray Santana-Falcón⁴, Chris D. Jones^{5,7}

6
7 ¹NORCE Norwegian Research Centre & Bjerknes Centre for Climate Research, Bergen, Norway

8 ²Department of Biology, Norwegian University of Science and Technology, Trondheim, Norway

9 ³Canadian Centre for Climate Modelling and Analysis, Environment and Climate Change Canada,
10 Victoria, BC, Canada

11 ⁴CNRM, Université de Toulouse, Meteo-France, CNRS, Toulouse, France

12 ⁵Met Office Hadley Centre, Exeter, United Kingdom

13 ⁶Research Institute for Global Change, Japan Agency for Marine-Earth Science and Technology,
14 Yokohama 236-0001, Japan

15 ⁷[School of Geographical Sciences, University of Bristol, UK](#)

16
17 *Corresponding author, ali.asaadi@mail.mcgill.ca

18
19 **Abstract**

20 Limiting global warming to well below 2°C by the end of the century is an ambitious target that requires
21 immediate and unprecedented emission reductions. In the absence of sufficient near term mitigation,
22 this target will only be achieved by carbon dioxide removal (CDR) from the atmosphere later during this
23 century, which would entail a period of temperature overshoot. Next to the socio-economic feasibility
24 of large-scale CDR, which remains unclear, the effect on biogeochemical cycles and climate are key to
25 assessing CDR as a mitigation option. Changes in atmospheric CO₂ concentration and climate alter the
26 CO₂ exchange between the atmosphere and the underlying carbon reservoirs of land and the ocean.
27 Here, we investigate carbon cycle feedbacks under idealized and more realistic overshoot scenarios in
28 an ensemble of Earth system models. The response of oceanic and terrestrial carbon stocks to changes
29 in atmospheric CO₂ concentration and changes in surface climate (the carbon-concentration and
30 carbon-climate feedback, quantified by the feedback metrics β and γ , respectively) show a large
31 hysteresis. This hysteresis leads to growing absolute values of β and γ during phases of negative
32 emissions. We find that this growth over time occurs such that the spatial patterns of feedbacks do not
33 change significantly for individual models. We confirm that the β and γ feedback metrics are a
34 relatively robust tool to characterize inter-model differences in feedback strength since the relative
35 feedback strength remains largely stable between phases of positive and negative emissions and
36 between different simulations, although exceptions exist. When emissions become negative, we find
37 that the model uncertainty (model disagreement) in β and γ increases stronger than expected from
38 the assumption that the uncertainties would accumulate linearly with time. This indicates that the
39 model response to a change from increasing to decreasing forcing introduces an additional layer of
40 uncertainty, at least in idealized simulations with a strong signal. We also briefly discuss the existing
41 alternative definition of feedback metrics based on instantaneous carbon fluxes instead of carbon
42 stocks and provide recommendations for the way forward and future model intercomparison projects.

Deleted: 1.5

Deleted: is spatially quite homogeneous, since

45 **1. Introduction**

46 Estimated remaining carbon budgets compatible with limiting anthropogenic warming to 1.5 or 2 °C
47 above pre-industrial levels are extremely tight and will be exhausted within the next few years if the
48 current emission rate is maintained (e.g., Rogelj et al. 2015; Goodwin et al. 2018; V. Masson-Delmotte
49 et al. 2018; Forster et al. 2023; Smith et al. 2023). Therefore, unless CO₂ emissions are reduced
50 immediately at an unprecedented rate, the 1.5 or 2°C targets can only be reached after a period of
51 temperature overshoot (Rogelj et al. 2015; Ricke et al. 2017; Geden and Löschel 2017; Riahi et al. 2021).
52 Although the option to remove large quantities of carbon from the atmosphere remains speculative
53 (Gasser et al. 2015; Larkin et al. 2018; Fuss et al. 2018; Creutzig et al. 2019; Smith et al. 2023), in such
54 overshoot pathways, too large near-term carbon emissions would be compensated by large-scale
55 carbon dioxide removal (CDR) later in this century. Research on negative emissions exploring the
56 reversibility of CO₂-induced climate change has been conducted for more than a decade (e.g., Boucher
57 et al. 2012; Wu et al. 2015; Tokarska and Zickfeld 2015; Li et al. 2020; Jeltsch-Thömmes et al. 2020;
58 Yang et al. 2021; Schwinger et al. 2022; Bertini and Tjiputra 2022). These studies generally report a
59 hysteresis behavior of the Earth system under negative emission, resulting in greatly varying
60 reversibility for different aspects of the Earth system. While the surface temperature trend follows a
61 reduction in atmospheric CO₂ relatively closely (e.g., Boucher et al. 2012; Jeltsch-Thömmes et al. 2020),
62 hysteresis can be large in the interior ocean, making for example ocean heat content and steric sea
63 level rise as well as interior ocean oxygen content and acidification largely irreversible on policy relevant
64 timescales (Mathesius et al. 2015; Li et al. 2020; Schwinger et al. 2022; Bertini and Tjiputra 2022). The
65 same is true for the loss of carbon from thawing permafrost soils (MacDougall et al. 2015; Gasser et al.
66 2018; Park and Kug 2022; Schwinger et al. 2022).

67 Carbon emissions drive multiple responses of the Earth system via changes in its physical climate and
68 the biogeochemical carbon cycle. Under increasing atmospheric CO₂ concentrations, increasing carbon
69 uptake by the ocean and terrestrial biosphere slows down global climate change by removing the
70 greenhouse gas CO₂ from the atmosphere, a process that is mainly driven by the dissolution of CO₂ into
71 the oceans (e.g., Revelle and Suess 1957, Siegenthaler and Oeschger 1978) and the CO₂-fertilisation
72 effect on the terrestrial biosphere (Schimel et al. 2015). On the other hand, Earth system model (ESM)
73 simulations show that this carbon uptake is reduced by progressive global warming due to, among
74 others, changes in ocean circulation and a reduction of CO₂ solubility in warmer waters, as well as
75 increased respiration rates from soils (Tharammal et al. 2019; Arora et al. 2020; Canadell et al. 2021),
76 and carbon release from degrading permafrost. These two feedback processes, the response to rising
77 CO₂ concentrations and the response to climate change, are termed carbon-concentration and carbon-
78 climate feedback, respectively (Gregory et al. 2009). In the context of overshoot pathways, carbon cycle
79 feedbacks determine the efficiency of negative emissions as the oceans and the terrestrial biosphere
80 will first take up carbon at reduced rates and eventually turn into sources of carbon to the atmosphere
81 (Jones et al. 2016a; Schwinger and Tjiputra 2018).

82 The carbon-concentration and carbon-climate feedbacks can be characterized by feedback metrics, for
83 example, by feedback factors β and γ (Friedlingstein et al. 2003) that quantify the gain/loss of carbon
84 in terrestrial or marine reservoirs per unit change in atmospheric CO₂ concentration and temperature,
85 respectively (see Section 2 for details). These feedback factors are valuable tools to compare the

Deleted: decades

Deleted: 2018

Deleted: Smith et al. 2016;

Deleted:)

Deleted: ,

Deleted: .

92 feedback strength among different models (Friedlingstein et al. 2003, 2006; Yoshikawa et al. 2008; Boer
93 and Arora 2009; Gregory et al. 2009; Roy et al. 2011; Arora et al. 2013, 2020) and can be calculated
94 using idealized model simulations, in which the effect of CO₂ on the carbon cycle and the radiative effect
95 of CO₂ are decoupled. In a biogeochemically coupled (BGC) simulation, the radiation code of an ESM
96 does not respond to increasing atmospheric CO₂ concentrations, but the terrestrial and marine carbon
97 cycles do. There is little climate change in such a simulation, which can therefore be used to quantify
98 the carbon-concentration feedback. The difference between a standard (fully coupled, COU) simulation
99 and the BGC simulation is used to quantify the carbon-climate feedback. In the last two phases of the
100 Coupled Model Intercomparison Project (CMIP5 and CMIP6, Taylor et al. 2012; Eyring et al. 2016)
101 carbon cycle feedbacks were addressed by conducting additional decoupled simulations of the standard
102 1% CO₂ simulation, which prescribes an increase in atmospheric CO₂ by 1% per year until quadrupling
103 (Arora et al. 2013, 2020). Next to this idealized simulation, the protocol for the CMIP6 Coupled Climate-
104 Carbon Cycle Model Intercomparison Project (C4MIP, Jones et al. 2016b) also proposes a BGC
105 simulation for the SSP5-3.4-OS (hereafter ssp534-over) scenario (O'Neill et al. 2016). This scenario
106 describes an overshoot pathway, in which emissions increase unmitigated until 2040, but strong
107 mitigation (including CDR) is undertaken thereafter. In contrast to the 1% CO₂ simulation, where no
108 forcing other than atmospheric CO₂ is varied, the quantification of feedbacks in this scenario simulation
109 is complicated by the presence of land use change and changes in radiative forcing through emissions
110 of aerosols and non-CO₂ greenhouse gasses (Melnikova et al. 2021, 2022).

Deleted: (1pctCO2 hereafter),

Deleted: 1pctCO2

111 One open question regarding carbon cycle feedbacks under negative emissions is relative to which state
112 the feedbacks should be measured. A sensible definition requires that any gain or loss of carbon is
113 calculated relative to a state where the carbon cycle is in equilibrium. Schwinger and Tjiputra (2018)
114 have opted to keep the pre-industrial state as the reference also after the onset of negative emissions.
115 We follow this approach here, but we note that recently Chimuka et al. (2023) proposed an alternative
116 approach, which defines the feedbacks during the negative emission phase relative to the state at the
117 onset of negative emissions. Since, the Earth system will be in disequilibrium at this point in time, this
118 approach requires an additional simulation that allows to estimate and remove the lagged response of
119 the Earth system to this disequilibrium.

120 Permafrost soils in the northern high latitudes have accumulated roughly 1100-1700 Pg of carbon in
121 the form of frozen organic matter, about twice as much as currently contained in the atmosphere
122 (Hugelius et al. 2014; Schuur et al. 2015). The release of CO₂ and methane (CH₄) from thawing
123 permafrost will amplify global warming due to anthropogenic emissions and further accelerate
124 permafrost degradation and microbial decomposition (Feng et al. 2020; Smith et al. 2022). This positive
125 feedback and the fact that Arctic temperatures are increasing at a much faster rate than the global
126 average (Liang et al. 2022; Rantanen et al. 2022) have made permafrost to be considered among the
127 key tipping elements of the climate system, although it may not be an abrupt but irreversible process
128 (Armstrong McKay et al. 2022; Yokohata et al. 2020; Lenton et al. 2019). A temporary temperature
129 overshoot might entail important legacy effects as high latitude ecosystems and the state of
130 permafrost-affected soils take several centuries to adjust to the new atmospheric condition (de Vrese
131 and Brovkin 2021). Current generation ESMs are still in their infancy when it comes to representing the
132 complex and often small-scale processes of permafrost carbon degradation. Here we take advantage
133 of the fact that one of the CMIP6 ESMs considered in this study has a vertically resolved representation

Deleted: twice as fast as

Deleted: Jenkins and Dai 2021;

Deleted:)

139 of soil carbon, which enables us to estimate the contribution of permafrost degradation to the total
140 carbon-climate feedback for this model.

141 Except for the recent studies by Schwinger and Tjiputra (2018), Melnikova et al. (2021, 2022), and
142 Chimuka et al. (2023) all previous studies that quantify carbon-concentration and carbon-climate
143 feedbacks are based on ESM simulations with increasing atmospheric CO₂. Here, we take advantage of
144 a simulation conducted for the CMIP6 Carbon Dioxide Removal Model Intercomparison Project
145 (CDRMIP, Keller et al. 2018) that mirrors the 1% CO₂ simulation by prescribing a decrease of
146 atmospheric CO₂ by 1% per year. For simplicity, we refer to these two simulations as 1pctCO₂-cdr in the
147 following text. We complement this simulation with a BGC simulation (1pctCO₂-cdr-bgc) to quantify, in
148 a manner consistent with previous feedback studies (Arora et al. 2013, 2020), carbon-concentration
149 and carbon-climate feedbacks under negative emissions in an ensemble of CMIP6 ESMs. We
150 complement these previous studies by a spatial analysis of feedback patterns, and compare the
151 feedbacks from the positive and negative emission phases of the 1pctCO₂-cdr simulation to the
152 feedbacks obtained from the ssp534-over scenario. For the latter, land use change has been shown to
153 have a dominant effect over carbon-concentration or carbon-climate feedbacks by Melnikova et al.
154 (2021, 2022), and these authors present a more detailed analysis of the role of land use change in the
155 ssp534-over scenario. Since land use change is not a feedback process, we focus in this study on regions
156 that are not dominated by agricultural areas when comparing feedbacks between the ssp534-over and
157 1pctCO₂-cdr simulations.

158 The purpose of this study is to investigate the evolution of carbon cycle feedbacks and their uncertainty
159 under deployment of negative emissions. Since feedback metrics are known to depend on the emission
160 (or concentration) pathway, we investigate the relative feedback strength and the spatial patterns of
161 feedbacks between positive and negative emission phases as well as between idealized and scenario
162 simulations. We also briefly explore the contribution of permafrost carbon losses to the carbon-climate
163 feedback and the impact of alternative feedback metric definitions that rely on instantaneous carbon
164 fluxes rather than carbon stocks in the context of negative emissions.

165

166 2. Description of feedback metrics, simulations, and models

167 2.1 Carbon cycle feedback metrics

168 The sensitivity of the carbon cycle to changes in atmospheric CO₂ concentration ([CO₂]) and its
169 sensitivity to changes in physical climate can be measured using two feedback metrics, which can be
170 based on either changes in carbon stocks (as introduced by Friedlingstein et al., 2003) or instantaneous
171 carbon fluxes (as introduced by Boer and Arora 2009). Changes in carbon stocks are equivalent to the
172 time-integrated carbon fluxes across the air-land and air-sea interfaces, such that for the Friedlingstein
173 et al. approach (referred to as integrated flux-based approach), the two feedback metrics are:

- 174 1. β (PgC/ppm), which quantifies the strength of the carbon-concentration feedback, i.e., the
175 changes in oceanic and terrestrial carbon stocks ($\Delta C_{L,O}$) in response to changes in atmospheric
176 CO₂ concentration ($\Delta[CO_2]$), and

Deleted: and

Deleted: 1pctCO2

Deleted: (

Deleted:).

Deleted: and 1pctCO2

Deleted: simulations

Deleted: SSP5-3.4-OS

Deleted: SSP5-3.4-OS

Deleted: SSP5-3.4-OS

186 2. γ (PgC/°C), which measures the strength of the carbon-climate feedback, i.e., changes in land
 187 and ocean carbon stocks ($\Delta C_{L,O}$) in response to changes in global average surface temperature
 188 (ΔT), where ΔT serves as a proxy for climate change.

189 Carbon feedback analysis requires, in addition to a standard fully coupled (COU) simulation, a
 190 biogeochemically (BGC) coupled simulation. In a BGC simulation, atmospheric $[\text{CO}_2]$ is kept constant at
 191 its pre-industrial values for the radiative transfer calculations, to isolate the response of land and ocean
 192 biogeochemistry to rising $[\text{CO}_2]$ in the absence of CO_2 -induced climate change. Using this pair of
 193 simulations (COU and BGC) results in the following expressions for β and γ (see Schwinger et al. 2014
 194 for a derivation).

$$195 \quad \beta_x = \frac{1}{\Delta[\text{CO}_2]} \left(\frac{\Delta C_x^{\text{BGC}} \Delta T^{\text{COU}} - \Delta C_x^{\text{COU}} \Delta T^{\text{BGC}}}{\Delta T^{\text{COU}} - \Delta T^{\text{BGC}}} \right)$$

$$196 \quad \approx \frac{\Delta C_x^{\text{BGC}}}{\Delta[\text{CO}_2]} \quad (1)$$

$$198 \quad \gamma_x = \frac{\Delta C_x^{\text{COU}} - \Delta C_x^{\text{BGC}}}{\Delta T^{\text{COU}} - \Delta T^{\text{BGC}}}$$

$$199 \quad \approx \frac{\Delta C_x^{\text{COU}} - \Delta C_x^{\text{BGC}}}{\Delta T^{\text{COU}}} \quad (2)$$

200 where X can be either L for land or O for ocean. Although there is no change in the radiative forcing of
 201 CO_2 in the BGC simulation (such that we could expect $\Delta T^{\text{BGC}} = 0$), surface temperature can vary due
 202 to changes in other radiative forcing agents (aerosols and non- CO_2 greenhouse gases). Even in the
 203 idealized 1pct CO_2 -cdr simulation, where CO_2 is the only variable forcing, there are some climatic
 204 changes over the land surface due to a reduction in latent heat fluxes associated with stomatal closure
 205 at higher CO_2 levels, as well as changes in vegetation structure, coverage, and composition (Arora et al.
 206 2020), which result in a small temperature increase along with changes in precipitation and soil
 207 moisture. The assumption of $\Delta T^{\text{BGC}} = 0$ will simplify equations (1) and (2) such that the rightmost term
 208 holds. However, results presented here are calculated using the complete expression for β and γ
 209 (without the assumption $\Delta T^{\text{BGC}} = 0$), unless otherwise noted. For comparison, we also provide
 210 feedback factors calculated using the simplified (rightmost) definition of β and γ in some figures. The
 211 instantaneous flux-based approach is equivalent to equations (1) to (2) except that the deviation of the
 212 carbon pools ΔC_x are replaced by the instantaneous air-sea or air-land carbon fluxes F_x . To distinguish
 213 these feedback metrics from the integrated flux-based ones, the capital letters B and Γ are used to
 214 denote them. The units of B and Γ are $\text{PgCyr}^{-1}\text{ppm}^{-1}$ and $\text{PgCyr}^{-1}\text{°C}^{-1}$, respectively.

Deleted: gasses

216 By combining equations (1) and (2) to yield

$$217 \quad \beta_x = \frac{1}{\Delta[\text{CO}_2]} (\Delta C_x^{\text{BGC}} - \gamma_x \Delta T^{\text{BGC}}) \quad (3)$$

218 it can be seen that, in order to calculate β_x , the carbon stock changes in the biogeochemically coupled
 219 simulation are corrected for global mean temperature changes using γ_x . Hence, temperature changes
 220 in the biogeochemically coupled simulation are fully accounted for as long as the underlying assumption
 221 of linearity holds. However, this assumption might be problematic, for example, if the spatial pattern
 222 of warming in a biogeochemically coupled scenario simulation arising from non- CO_2 forcings is very

different from the warming patterns in the fully coupled simulation, particularly if the sign of the local temperature change is different from the global average (e.g., local cooling vs. global average warming). Such effects could become important on regional to local scales and will be discussed in Section 3.4.

It is worth mentioning that these feedback frameworks should be seen as a technique for assessing the relative sensitivities of models and understanding their differences (i.e. the model uncertainty of the estimated feedbacks), rather than as absolute measures of invariant system properties (Gregory et al. 2009; Ciais et al. 2013). The values of carbon cycle feedback metrics can vary over time within a model simulation (e.g., Arora et al. 2013) or between different scenarios (Hajima et al. 2014).

To gain insight into the reasons for differing responses among models, we apply the decomposition of the simplified expression for β_L (Eq. 1, assuming $\Delta T^{BGC} = 0$) following Arora et al. (2020). This allows us to investigate the contributions from different processes to changes in vegetation and soil carbon reservoirs (ΔC_V and ΔC_S , respectively).

$$\beta_L = \frac{\Delta C_L^{BGC}}{[CO_2]} = \frac{\Delta C_V^{BGC} + \Delta C_S^{BGC}}{[CO_2]} = \left(\frac{\Delta C_V^{BGC}}{\Delta NPP^{BGC}} \frac{\Delta NPP^{BGC}}{\Delta GPP^{BGC}} \frac{\Delta GPP^{BGC}}{[CO_2]} \right) + \left(\frac{\Delta C_S^{BGC}}{\Delta R_h^{BGC}} \frac{\Delta R_h^{BGC}}{\Delta LF^{BGC}} \frac{\Delta LF^{BGC}}{[CO_2]} \right)$$

$$= \tau_{cveg\Delta} \frac{\Delta GPP^{BGC}}{[CO_2]} + \tau_{csoil\Delta} \frac{\Delta R_h^{BGC}}{\Delta LF^{BGC}} \frac{\Delta LF^{BGC}}{[CO_2]} \quad (4)$$

ΔNPP , ΔGPP , ΔR_h , and ΔLF represent deviations of the net primary productivity, gross primary productivity, heterotrophic respiration, and litterfall flux, respectively, from their pre-industrial values. The terms $\tau_{cveg\Delta}$ and $\tau_{csoil\Delta}$ are turnover times (in years) of carbon in the vegetation and litter plus soil pools. $\frac{\Delta NPP}{\Delta GPP}$ is a measure of carbon use efficiency for the fraction of GPP (above its pre-industrial value) that turned into NPP after subtracting autotrophic respiration losses (denoted as CUE Δ). $\frac{\Delta GPP}{[CO_2]}$ (PgCyr $^{-1}$ ppm $^{-1}$) and $\frac{\Delta R_h}{\Delta LF}$ are a measure of the global CO $_2$ fertilization effect and the increase in heterotrophic respiration per unit increase in litterfall rate, respectively. Also, $\frac{\Delta LF}{[CO_2]}$ (PgCyr $^{-1}$ ppm $^{-1}$) measures the global increase in litterfall rate per unit increase in CO $_2$.

2.2 Model simulations

The 1% CO $_2$ experiment is a highly idealized model experiment that prescribes a rate of 1% per year increase in [CO $_2$] from pre-industrial values until quadrupling after 140 years. No other forcings are varied in this experiment, i.e., land use as well as non-CO $_2$ greenhouse gasses and aerosol concentrations are held constant at their pre-industrial levels. This experiment has already been performed by the first coupled atmosphere-ocean general circulation models in the late 1980s, and important climate metrics such as the transient climate response (TCR; Meehl et al. 2020) and the transient response to cumulative emissions (TCRE; e.g., Gillett et al. 2013) are formally defined through the 1pctCO $_2$ simulation. Likewise, the C4MIP carbon cycle feedback analysis for the last two phases of CMIP (Arora et al. 2013, 2020) relied on this simulation. Given the importance of the 1% CO $_2$ experiment, the CMIP6 CDRMIP protocol proposes an experiment that mirrors this simulation by

Deleted: idealized

Deleted: Therefore, the

Deleted: .

Deleted: 3

Deleted: 1pctCO2

Deleted: .

Deleted: 1pctCO2

Deleted: the 1pctCO2

268 starting from its endpoint at year 140 and decreasing atmospheric CO₂ at a rate of 1% per year until
269 pre-industrial [CO₂] is restored. This experiment is designed to investigate the response of the Earth
270 system to carbon dioxide removal in an idealized fashion. As noted above, in this study we refer to the
271 1% CO₂ simulation and the mirrored -1% CO₂ CDRMIP simulation collectively as 1pctCO₂-cdr for
272 simplicity. We note that the implied rates of CDR in the 1pctCO₂-cdr simulation are huge and not
273 practically feasible. Also, there is a jump from very large positive to very large negative diagnosed
274 emissions at the end of year 140, which is clearly unrealistic. To investigate carbon cycle feedbacks
275 under CDR, we have complemented the 1pctCO₂-cdr simulation with a biogeochemical coupled
276 1pctCO₂-cdr-bgc simulation that starts from the endpoint of the 1pctCO₂-bgc simulation at year 140.

Deleted: (1pctCO2-cdr).

277 The family of Shared Socioeconomic Pathways (SSPs, O'Neill et al. 2014) is designed to represent
278 different socio-economic futures that social, demographic, political, and economic developments could
279 lead to. These narrative SSPs are the basis for a set of quantitative future scenarios, a selection of which
280 is now being used as input for scenario simulations by the latest ESMs in the frame of the CMIP6
281 ScenarioMIP (O'Neill et al. 2016). The ssp534-over scenario follows the high emission SSP5-8.5 pathway
282 until 2040 at which point strong mitigation policies are introduced to rapidly reduce emissions to zero
283 by about 2070 and to net-negative levels thereafter (Fig. 3 of O'Neill et al. 2016). In contrast to the
284 1pctCO₂-cdr simulation, the ssp534-over scenario includes land use change as well as time varying
285 forcing from aerosols and non-CO₂ greenhouse gasses throughout the simulation period (Fig. 1 of
286 Liddicoat et al. 2021). For this study, we use the 1pctCO₂-cdr and ssp534-over simulations from the
287 CMIP6 archive together with the corresponding biogeochemically coupled simulations of these
288 experiments. We note that the biogeochemically coupled 1pctCO₂-cdr-bgc experiment is not part of
289 CMIP6, but has been performed for this study by participating modelling groups.

Deleted: SSP5-3.4-O5

Deleted: SSP5-3.4-O5

Deleted: , 1pctCO2

Deleted: ,

Deleted: SSP5-3.4-O5

290 The C4MIP simulation protocol does not allow to separate carbon release (or uptake) through land use
291 changes from the carbon-concentration feedback, since land use is active in the biogeochemically
292 coupled ssp534-over simulation. To focus on carbon cycle feedbacks, we eliminate the effect of land
293 use changes as much as possible by identifying regions that are mostly unaffected by human activity
294 (referred to as "natural land"). To accomplish this in a way that available CMIP6 output permits, we
295 define natural land as grid cells with a maximum cropland fraction of less than 25% at all time steps
296 during the period 2015-2100. The threshold of 25% used here for our heuristic approach is a
297 compromise between accuracy (some signal of land use change is still present) and spatial coverage
298 (with increasingly lower thresholds, larger areas of the globe are excluded). Our results are not very
299 sensitive to variations in the threshold between approximately 10 and 30%. Maps of maximum ssp534-
300 over cropland fraction for each model (Fig. S1) indicates that a 25% threshold reasonably identifies
301 hotspots of agricultural production. To make our analysis comparable between the ssp534-over and
302 1pctCO₂-cdr simulations, we use the same set of grid cells also for the 1pctCO₂-cdr simulation (unless
303 otherwise noted), even though land cover is not changed from its pre-industrial state in this simulation.
304 We acknowledge that our approach does not explicitly address pasture gridcells or transition from other
305 land use types to pasture. Nonetheless, in the ssp534-over scenario, a substantial expansion of
306 bioenergy crops between 2040 and 2070 is assumed to replace pasture areas, while the area of land
307 used as pasture remains relatively stable thereafter (see O'Neill et al. 2016). Hence, our approach, for
308 this specific scenario, captures the majority of gridcells with transitions from pasture to cropland, while
309 transitions from pasture to forest remain small.

Deleted: SSP5-3.4-O5

Deleted: (over the period 2015 to 2100) crop-land

Deleted: %.

Deleted: ,

Deleted: SSP5-3.4-O5

Deleted: SSP5-3.4-O5

322

323 **2.3 Participating Earth System Models**

324 Table 1 summarizes the five ESMs that contributed to this study along with the experiments used for
 325 the analyses presented here. The primary features of these models are listed in Table 2 of Arora et al.
 326 (2020). MIROC-ES2L, NorESM2-LM (which employs version 5 of the Community Land Model, CLM5),
 327 and UKESM1-0-LL have a representation of the terrestrial nitrogen cycle implemented and coupled to
 328 their carbon cycle. Only the UKESM1-0-LL model has a land component that dynamically simulates
 329 vegetation cover and competition between their plant functional types (PFTs). Fire is included in the
 330 CNRM-ESM2-1 and NorESM2-LM models. NorESM2-LM is the only ESM with vertically resolved soil
 331 carbon, which allows studying the impact of warming on the carbon stored in permafrost soils in more
 332 detail. In this study, a gridcell was considered permafrost where the pre-industrial maximum active
 333 layer thickness was shallower than three meters. [A description and a comparison of the ocean
 334 biogeochemistry models used in the five ESMs can be found in the review of Séférian et al. \(2020\).](#)

Deleted: ,

Deleted: the

336 **Table 1:** List of CMIP6 ESMs used in this study, names of their biogeochemical component models, resolution
337 and experiment variants used.

	CanESM5	CNRM-ESM2-1	MIROC-ES2L	NorESM2-LM	UKESM1-0-LL
Atmosphere and land resolution	2.81°x2.81°*	1.4°x1.4°	2.81°x2.81°	1.9°x2.5°	1.875°x1.25°
variant	r1i1p1f1 & r1i1p2f1*	r1i1p1f2	r1i1p1f2	r1i1p1f1	r4i1p1f2 & r1i1p1f2
Ocean resolution	1° (finer in the tropics)	1° (finer in the tropics)	1° (finer close to North Pole and Equator)	1° (finer near the Equator)	1°
Ocean biogeochemistry model name	CMOC (biology); carbonate chemistry follows OMIP protocol	PISCESv2-gas	OECO2	iHAMOCC	MEDUSA-2.1
Land model name	CLASS-CTEM	ISBA-CTRIP	MATSIRO (physics), VISIT-e (BGC)	CLM5	JULES-ES-1.0
Reference	Swart et al. (2019)	Séférián et al. (2019)	Hajima et al. (2020)	Tjiputra et al. (2020); Seland et al. (2020)	Sellar et al. (2019)

338 *CMIP6 experiment variant used across different simulations including: piControl, historical, hist-bgc, ssp585, ssp585-bgc,
339 ssp534-over, ssp534-over-bgc, 1pctCO₂, 1pctCO₂-bgc, 1pctCO₂-cdr, and 1pctCO₂-cdr-bgc experiments.

340

343 **3. Results and Discussion**

344 **3.1 Atmospheric CO₂, temperature, and carbon fluxes**

345 The atmospheric CO₂ concentration ([CO₂]) for the concentration-driven [ssp534-over](#) scenario peaks at
346 571 ppm (a doubling of pre-industrial CO₂ concentration) in the year 2062 and decreases to 497 ppm
347 in 2100 (Fig. 1a). According to the scenario design (see O'Neill et al. 2016), strong mitigation policies
348 (including deployment of bioenergy with carbon capture and storage (BECCS) and other carbon dioxide
349 removal technologies) start in 2040 resulting in an immediate decrease in the CO₂ growth rate that
350 peaks in 2041 (Fig. 1e). In the [1pctCO₂-cdr](#) simulation, the prescribed [CO₂] is symmetric around its
351 4xCO₂ peak of 1133 ppm in the year 140 (Fig. 1c). The rate of change of the CO₂ concentration (Fig. 1e)
352 is very different between [ssp534-over](#) and [1pctCO₂-cdr](#) experiments. In particular, the CO₂ growth rate
353 in the idealized [1pctCO₂-cdr](#) experiment has a sudden and large jump from positive to negative values
354 at the transition from the ramp-up to the ramp-down phase.

355 The five participating ESMS show large differences in global mean surface air temperature change,
356 relative to pre-industrial values, under the [ssp534-over](#) simulation (Fig. 1b). Peak temperatures vary
357 from 2°C in NorESM2-LM to 4.35°C in CanESM5. The timing of the global surface air temperature peak
358 varies from 2062 for the MIROC-ES2L and UKESM1-0-LL models to 2100 for CNRM-ESM2-1. After this
359 peak, the temperature declines again (except for CNRM-ESM2-1) reaching end-of-the-century values
360 that range from 1.39°C above pre-industrial in NorESM2-LM to 3.47°C in CanESM5. The multi-model
361 mean global surface air temperature is 2.66°C at the end of the 21st century. The model-mean growth
362 rate of the global surface air temperature (Fig. 1f) [plateaus](#) at about 0.05°C/yr between approximately
363 2030-2050 before it starts to decline to below zero towards the end of the simulation.

364 Temperature changes in the BGC simulation of [ssp534-over](#) are not negligible since the non-CO₂ forcing
365 agents as well as land use change do evolve in time in this scenario, in contrast to the idealized [1pctCO₂-](#)
366 [cdr](#) simulation. Positive peak temperature anomalies range from 0.37°C (CNRM-ESM2-1 in 2098) to
367 1.29°C (CanESM5 in 2057). UKESM1-0-LL also shows a pronounced negative temperature anomaly
368 during the historical period of the BGC simulation of -0.80°C in the year 1990.

Deleted: SSP5-3.4-05

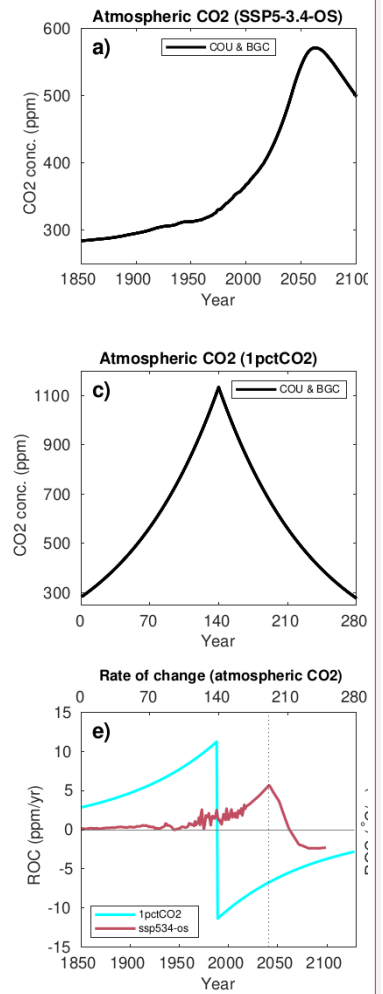
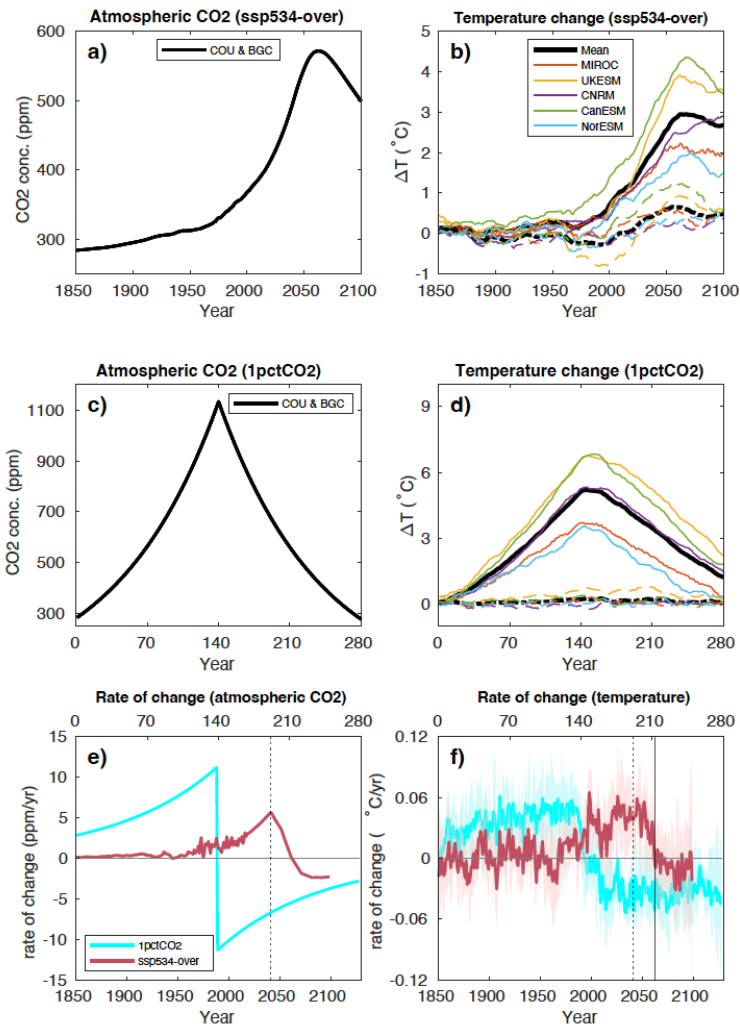
Deleted: ,

Deleted: SSP5-3.4-05

Deleted: SSP5-3.4-05

Deleted: plateaus

Deleted: SSP5-3.4-05



Deleted:

Deleted: SSP5-3.4-OS

Deleted: SSP5-3.4-OS

375
 376 **Figure 1:** Atmospheric CO₂ concentration and surface air temperature changes in the fully coupled (solid
 377 lines) and biogeochemically coupled (dashed lines) configurations of the *ssp534-over* (a,b) and *1pctCO₂-*
 378 *cdr* (c,d) experiments. The rates of change in the prescribed atmospheric CO₂ concentrations is shown
 379 in panel e, and the model mean rate of surface temperature change from the fully coupled simulations
 380 is shown in panel f. The dotted (solid) vertical lines in panels e and f indicate the peak of the CO₂ growth
 381 rate (CO₂ concentration) in the *ssp534-over* scenario. Shadings in panel f show the range across the
 382 models. An 11-year moving average has been used in panels b, d, and f.

386
387 In the 1pctCO₂-cdr simulation, the peak temperature anomalies vary from 3.57°C (in year 144) in
388 NorESM2-LM to 6.84°C (in year 151) in CanESM5 (Fig. 1d). Thereafter, temperature anomalies decline
389 to values ranging from 0.29°C in NorESM2-LM to 2.2°C in UKESM1-0-LL at the end of the ramp-down
390 period (year 280). The 1pctCO₂-cdr BGC simulation shows, compared to the ssp534-over BGC
391 simulation, smaller temperature anomalies ranging from -0.22°C (CNRM-ESM2-1 in year 149) to 0.79°C
392 (UKESM1-0-LL in year 207). The relatively large magnitude of the temperature anomaly in the ssp534-
393 over-bgc simulation (peak warming of 12% - 29% of the peak warming in the fully coupled simulation)
394 suggests that warming due to non-CO₂ forcings might contribute substantially to the carbon-climate
395 feedback in the ssp534-over scenario.

396 For atmosphere-land fluxes, our analysis is complicated by the fact that land use changes are present
397 in the ssp534-over scenario. Here, we focus on comparing fluxes and feedbacks for grid cells that are
398 dominated by “natural land” (see Sec. 2.2 for more details). Note that, for comparability, we consider
399 the same set of grid cells in the 1pctCO₂-cdr simulation, even though land cover stays at its pre-
400 industrial state in this simulation. In the ssp534-over simulations, the model-mean annual CO₂ fluxes
401 (Fig. 2) continue rising until the rate of change of [CO₂] reaches its peak in 2041. After the peak,
402 atmosphere-land and atmosphere-ocean fluxes start to decline rapidly in all models with little time lag.
403 UKESM1-0-LL and MIROC-ES2L simulate negative fluxes (i.e., natural land turns into a carbon source)
404 before the end of the 21st century in the COU simulation (Fig. 2a). Without the effect of CO₂ induced
405 warming (BGC simulation, Fig. 2b), only MIROC-ES2L shows a significant carbon source from the
406 terrestrial biosphere before 2100, while the model-mean still shows a sink. In the fully coupled 1pctCO₂-
407 cdr experiment, sink-to-source transition of the terrestrial biosphere occurs around year 165 in the
408 model mean, 25 years after the rate of change of [CO₂] peaks (Fig. 2c). Consistent with what is seen in
409 the biogeochemically coupled ssp534-over, the sink-to-source transition occurs 10 years later without
410 the effect of warming in the 1pctCO₂-cdr-bgc experiment. However, the terrestrial CO₂ source at the
411 end of the biogeochemically coupled 1pctCO₂-cdr simulation is larger than in the fully coupled
412 simulation. We also observe that models which take up more (less) terrestrial carbon during the CO₂
413 ramp-up phase release more (less) carbon towards the end of the CO₂ ramp-down phase (1pctCO₂-cdr-
414 bgc; Fig. 2c,d), indicating that these models have a larger (smaller) sensitivity ($\Delta C_i / \Delta CO_2$) to both
415 atmospheric CO₂ increase and decrease. We therefore interpret the increased source of carbon at the
416 end of the 1pctCO₂-bgc simulation as a release of additional carbon that has been taken up in the
417 absence of climate warming during the biogeochemically coupled simulation. The net negative emission
418 phase of the ssp534-over scenario is too short to show this effect in 2100 (where the warming effect
419 still reduces the model mean terrestrial carbon sink).

420 Likewise, the warming of the world's oceans in both simulations tends to reduce the carbon uptake or
421 increase the oceanic carbon source. The model spread for atmosphere-ocean carbon fluxes (Fig. 2,
422 panels e to h) appears to be much smaller than for the atmosphere-land fluxes. In the ssp534-over
423 simulation, the ocean remains a sink of carbon in all models until the end of the simulation in 2100. In
424 the 1pctCO₂-cdr simulation the ocean turns into a source of CO₂ to the atmosphere around year 175,
425 and in the BGC simulation without warming this transition is delayed by 7 years.

Deleted: SSP5-3.4-O5

Deleted: smaller

Deleted: BGC

Deleted: SSP5-3.4-O5 scenario compared to the 1pctCO₂-BGC simulations (also given the much higher CO₂ forcing

Deleted: latter

Deleted: a substantial part of

Deleted: SSP5-3.4-O5

Deleted: might be caused by non-CO₂ forcings

Deleted: SSP5-3.4-O5

Deleted: SSP5-3.4-O5

Deleted: natural

Deleted: SSP5-3.4-O5

Deleted: BGC

Deleted: (Fig. 2c,d)

Deleted: (1pctCO₂)

Deleted: .

Deleted: BGC

Deleted: an outgassing

Deleted: the excess

Deleted: could be

Deleted: .

Deleted: SSP5-3.4-O5

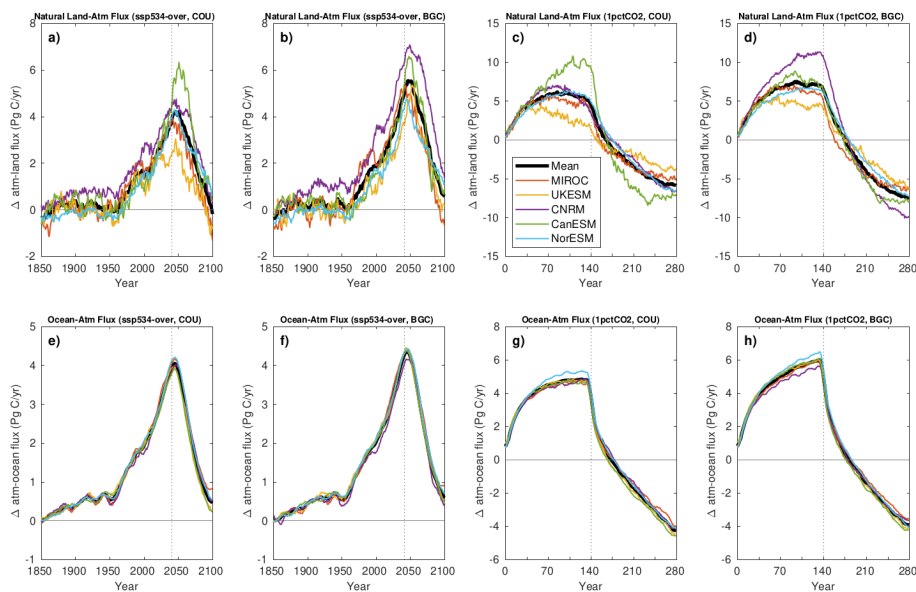
Deleted: increases

Deleted: source

Deleted: .

Deleted: SSP5-3.4-O5

426



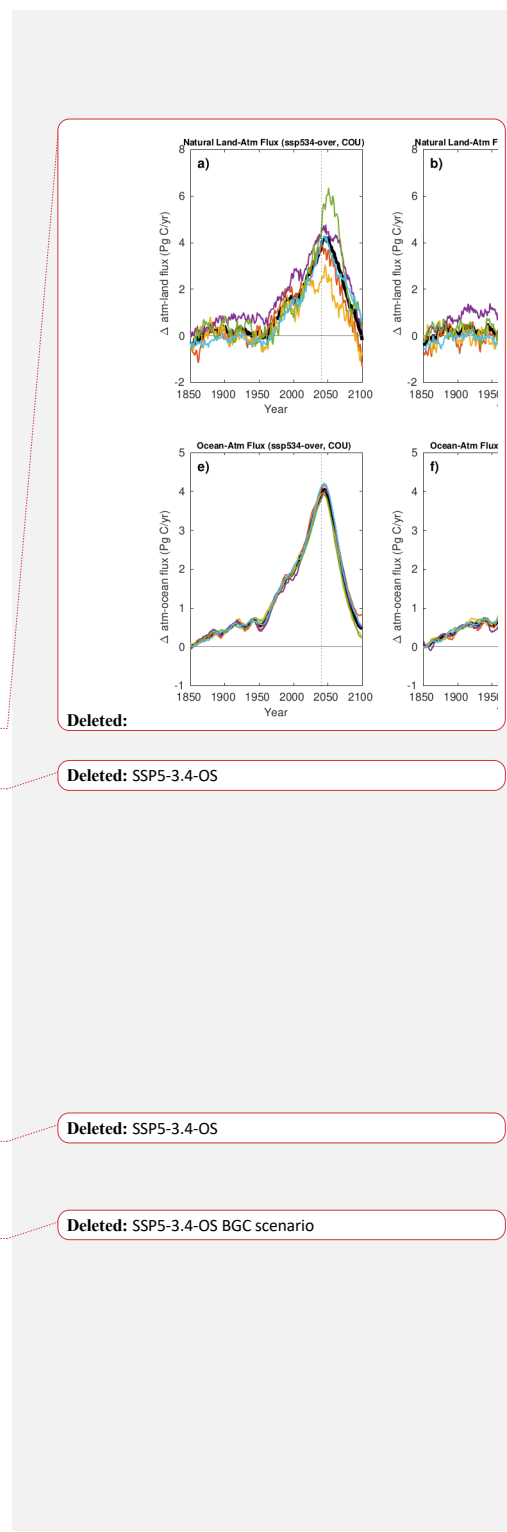
454
 455 **Figure 2:** Time series of annual mean natural atmosphere-land (a-d) and atmosphere-ocean (e-h)
 456 carbon fluxes for the fully and biogeochemically coupled ssp534-over and 1pctCO₂-cdr experiments as
 457 indicated in the panel titles. The dotted vertical lines indicate where [CO₂] growth rate peaks in each
 458 experiment. An 11-year moving average has been used in all panels.

459

460 3.2 Global mean carbon cycle feedbacks

461 3.2.1 Ocean

462 In the BGC simulation, where the effect of changing atmospheric CO₂ concentration on terrestrial and
 463 marine carbon uptake (the carbon-concentration feedback) is isolated, cumulative atmosphere-ocean
 464 carbon fluxes indicate an almost linear growth with [CO₂] as long as atmospheric CO₂ concentrations
 465 are increasing in both ssp534-over and 1pctCO₂-cdr simulations (Fig. 3a-c). When [CO₂] starts to decline,
 466 the atmosphere-ocean carbon flux in the 1pctCO₂-cdr simulation shows pronounced hysteresis with a
 467 continued ocean carbon uptake (until the [CO₂]-anomaly has been roughly reduced to 500 ppm) before
 468 starting to decrease towards the end of the ramp-down phase (Fig. 3b). In the ssp534-over-bgc
 469 simulation, where the onset of net negative emissions is more gradual, the relationship between
 470 cumulative atmosphere-ocean fluxes and [CO₂] during the phase of declining atmospheric CO₂
 471 concentration also shows hysteresis; but due to the relative short period of net-negative emissions, the
 472 ocean remains a sink of carbon in all models until the end of the simulation.



477 Differences in the cumulative atmosphere-ocean CO₂ flux between the COU and the BGC simulations
478 versus surface temperature changes (carbon-climate feedback) are shown in Fig. 3d-f. Increasing
479 temperature results in less carbon uptake by the ocean, except for the CNRM-ESM2-1 which simulates
480 slightly more uptake in the first half of the warming period under the [ssp534-over](#). During the negative
481 emission phases of the simulations when the air surface temperature is decreasing, the carbon-climate
482 feedback still decreases the ocean carbon content, albeit at reduced rates. Even when pre-industrial
483 CO₂ concentrations are restored at the end of the 1pctCO₂-cdr simulation all models agree that the
484 ocean is still losing carbon due to the effect of (legacy) warming (Fig. 3e). Using the global average
485 ocean potential temperature (averaged over the full ocean depth) instead of the surface air
486 temperature as a proxy for oceanic climate change as proposed by Schwinger and Tjiputra (2018), gives
487 a much more linear relationship between changes in the ocean carbon stock and changes in
488 temperature in the majority of models (Fig. 3 g-i). At the end of the [ssp534-over](#) and [1pctCO₂-cdr](#)
489 simulations, the ocean still holds a large part of the carbon taken up from the atmosphere since pre-
490 industrial time, between roughly 300-400 PgC in 1pctCO₂-cdr, and around 350 PgC in [ssp534-over](#) (Fig.
491 S2).

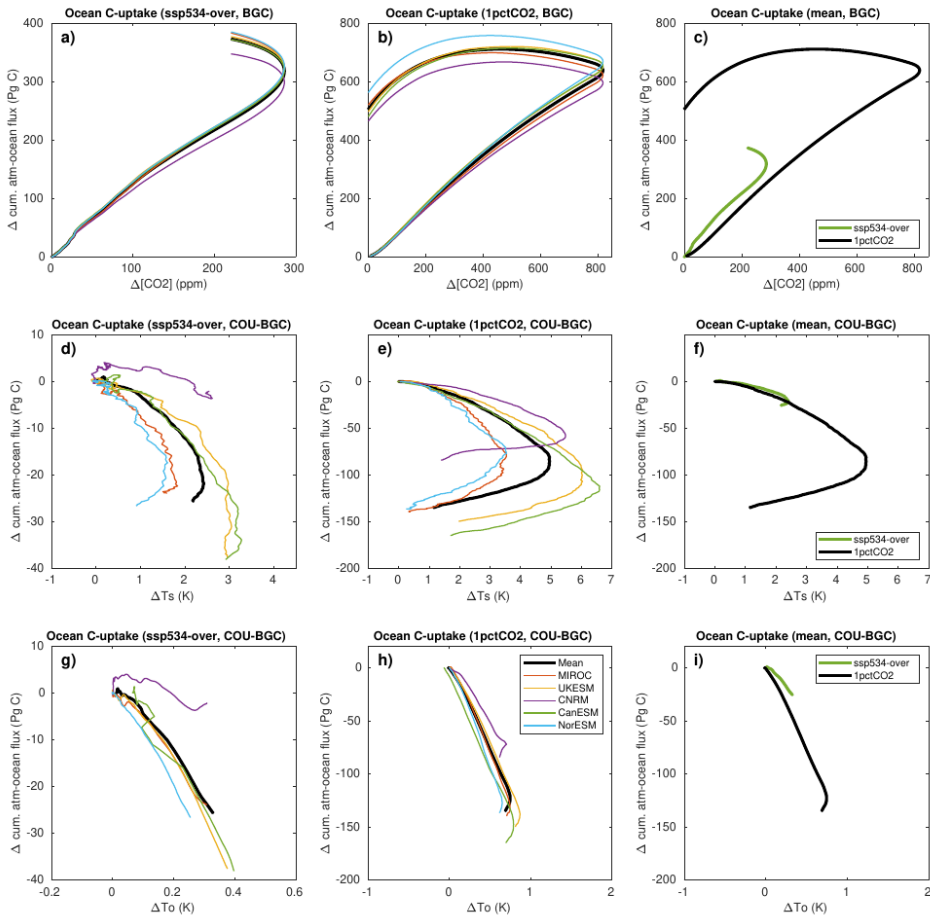
Deleted: SSP5-3.4-05

492 Generally, the ocean carbon-concentration feedback [\(as indicated by the cumulative carbon uptake per](#)
493 [unit increase of CO₂ concentration, Fig. 3a-c\)](#) is larger in the [ssp534-over](#) scenario, which can most likely
494 be explained with the slower growth rate of [CO₂] in this scenario compared to the 1pctCO₂-cdr
495 simulation (Fig. 3c). For slower growth rates, the ocean has more time to mix and partly transport the
496 adsorbed anthropogenic carbon away from the ocean surface to the interior, increasing the capacity
497 for more uptake. A larger carbon uptake at slower CO₂ growth rates has already been reported by
498 Gregory et al. 2009 and Hajima et al. 2014, although only for combined land and ocean fluxes or land
499 fluxes only. The ocean carbon-climate feedback, in contrast, is slightly smaller in the [ssp534-over](#)
500 scenario, i.e., the carbon loss for a given warming is smaller.

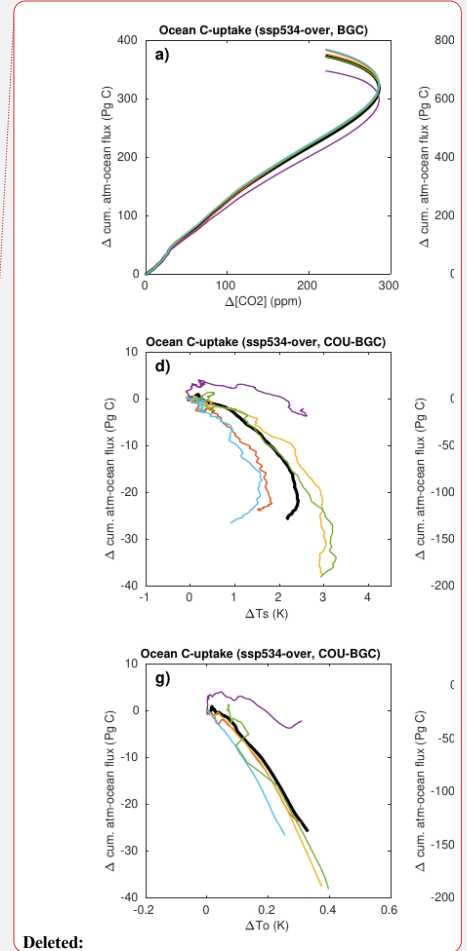
Deleted: SSP5-3.4-05

Deleted: SSP5-3.4-05

Deleted: SSP5-3.4-05

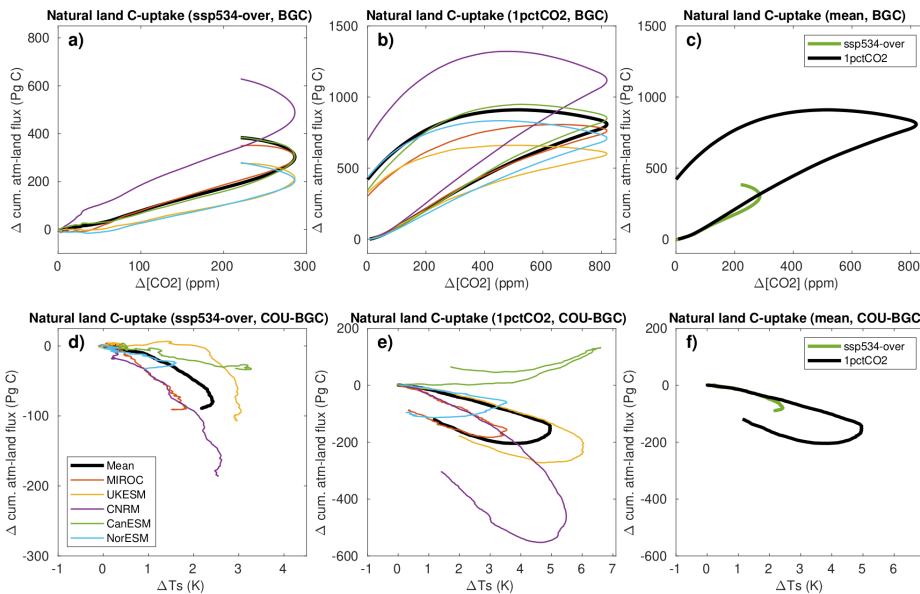


505
 506 **Figure 3:** Ocean carbon cycle feedbacks in the ssp534-over (left column) and 1pctCO₂-cdr (middle
 507 column) simulations for individual models. The model means for both simulations are shown in the
 508 right column. Global mean ocean potential temperature is used on the x-axis of panels (g-i). An 11-year
 509 moving average has been used in all panels.



Deleted:

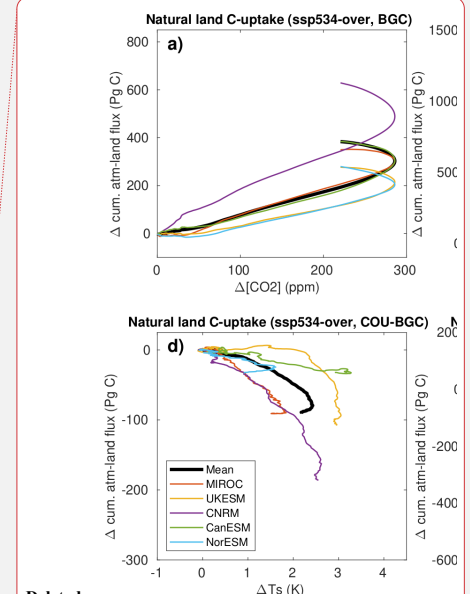
Deleted: SSP5-3.4-OS



517 **Figure 4:** Terrestrial carbon cycle feedbacks in the ssp534-over (left column) and 1pctCO₂-cdr (middle
 518 column) simulations for grid cells that are dominated by “natural land” (less than a maximum of 25%
 519 crop fraction over the period 2015-2100 in ssp534-over). Note that we consider the same grid cells in
 520 the 1pctCO₂-cdr simulation, even though land use stays at pre-industrial state. The model means for
 521 both simulations are shown in the right column. An 11-year moving average has been used in all panels.
 522
 523

524 3.2.2 Land

525 For grid cells representing natural land, the response of the cumulative terrestrial carbon flux to
 526 changes in [CO₂] and surface temperature (Fig. 4) is qualitatively similar to the response of the
 527 atmosphere-ocean fluxes. In both ssp534-over and 1pctCO₂-cdr simulations, a roughly linear
 528 relationship can be seen between the carbon flux change and both the changes in [CO₂] and surface air
 529 temperature during positive emission phases. An exception is the carbon-climate feedback of the
 530 CanESM5 model, which is about zero up to 4 degrees of warming, and becomes positive for higher
 531 temperature increases. This unique behavior is caused by CanESM5’s high climate sensitivity combined
 532 with larger carbon use efficiency amongst CMIP6 models (as shown later) which causes high latitude
 533 vegetation to take up large amounts of carbon in response to warming. This more than compensates
 534 for the carbon loss elsewhere associated with climate warming. During negative emission phases both
 535 feedbacks show a considerable hysteresis behavior, as for the ocean (see also below). It is worth
 536 mentioning that, unlike for the ocean, the COU-BGC accumulated atmosphere-land flux starts to
 537 increase, albeit with a lag, in response to cooling during the negative emissions phase in most models
 538 (Figs. 3e and 4e).



Deleted:

Deleted: SSP5-3.4-O5

Deleted: SSP5-3.4-O5

Deleted: SSP5-3.4-O5

543 The carbon-concentration feedback (as indicated by the cumulative carbon uptake per unit increase of
544 CO₂ concentration) is slightly smaller for the ssp534-over scenario compared to the 1pctCO₂-cdr
545 experiment (see Fig. 4c), but this difference might be attributed to the remaining influence of land-use
546 changes. This is because, for “cropland grid cells” (maximum crop-fraction of more than 25% in the
547 ssp534-over scenario), the cumulative carbon fluxes are markedly smaller in the ssp534-over scenario
548 compared to the 1pctCO₂-cdr simulation (compare panel c on Figs. S3 and 4). This indicates, consistent
549 with Melnikova et al. (2022) who demonstrate that carbon losses from land use changes dominate over
550 gains through CO₂ fertilization in crop dominated areas (see their Fig. 4, panels a and c), that the
551 prescribed land use change in the SSP scenario is the driver behind the small (negative for NorESM2-
552 LM and UKESM1-0-LL) carbon accumulation for crop land grid cells. Since grid cells that are dominated
553 by natural land according to our separation approach, may contain up to 25% croplands, we expect a
554 reduction of cumulative carbon fluxes due the remaining land use (changes) in the natural land grid
555 cells. We note that land use change is externally prescribed rather than a feedback process in our
556 simulations. It is only due to the simulation design used here (see Section 2.2 for details), that the
557 carbon release (or uptake) due to land use changes modifies the net atmosphere-land CO₂ flux which
558 is then seen as a carbon-concentration feedback in the ssp534-over-bgc simulation.

559 The model-mean carbon-climate feedback for natural land is very similar for the ssp534-over and
560 1pctCO₂-cdr simulations during the positive emission phases, but deviates thereafter due to hysteresis
561 behavior (Fig. 4f). Interestingly, in contrast to the carbon-concentration feedback, the model-mean
562 carbon-climate feedback for cropland and natural land remains very similar between the ssp534-over
563 and 1pctCO₂-cdr simulations (Fig. S3f). This is likely due to the similar response of the soil carbon to
564 changes in surface air temperature.

566 3.2.3 Hysteresis

567 For the 1pctCO₂-cdr simulation, hysteresis can be defined as the difference in, for example, cumulative
568 carbon uptake during the ramp-up and the ramp-down period at the same level of atmospheric CO₂
569 concentration. Here, to quantify hysteresis, we choose the years 70 and 210, which represent a state
570 where atmospheric CO₂ has been doubled (570 ppm) or returned to this value after the overshoot. We
571 define hysteresis as the difference between cumulative carbon uptake in year 210 minus cumulative
572 carbon uptake in year 70 (i.e., hysteresis is positive, if cumulative carbon uptake is larger on the ramp-
573 down side of the 1pctCO₂-cdr simulation). We refrain from quantifying hysteresis for the ssp534-over
574 scenario, because of the relatively short period of declining [CO₂].

575 The model mean hysteresis in the carbon-concentration feedback is 443±29 PgC (model uncertainty
576 measured as one standard deviation) for the ocean and 524±205 PgC for natural land, which for both
577 cases is larger than the feedback at year 70 itself. Although the hysteresis of the ocean carbon-
578 concentration feedback is smaller than the terrestrial feedback in absolute terms, it is larger in relative
579 terms (179% of the accumulated carbon uptake at year 70 for the ocean versus 168% for land). In
580 general, the hysteresis seems to be related to the magnitude of the carbon-concentration feedback,
581 since models with a large (small) carbon uptake at year 140, tend to show a large (small) hysteresis at

Deleted: SSP5-3.4-O5

Deleted: crop-land

Deleted: SSP5-3.4-O5

Deleted: SSP5-3.4-O5

Deleted: the results of

Deleted: UKESM

Deleted: not

Deleted: , and it obviously does not depend on atmospheric CO₂ concentration

Deleted: SSP5-3.4-O5-BGC

Deleted: SSP5-3.4-O5

Deleted: global average

Deleted: SSP5-3.4-O5

Deleted: S3

Deleted: SSP5-3.4-O5

597 year 210 for both ocean and land. However, towards the end of the ramp-down period, this relationship
598 breaks down for CanESM5 and MIROC-ES2L, particularly over land.

599 For the carbon-climate feedback, the hysteresis in climate induced carbon loss or gain (difference
600 between COU-BGC evaluated at years 70 and 210) is -102 ± 22 and -158 ± 181 PgC for ocean and natural
601 land, respectively. As for the carbon-concentration effect, a relationship between the magnitude of
602 carbon loss or gain at year 140 and the hysteresis is found. Models with a large (small) climate induced
603 loss of carbon tend to have a large (small) hysteresis.

604 For the ocean carbon cycle, hysteresis in the carbon-concentration feedback occurs mainly due to the
605 long time scales of ocean overturning circulation. Schwinger and Tjiputra (2018) have shown that
606 hysteresis strongly increases with water mass age. Young waters, which reside close to the ocean
607 surface, exchange quickly with the atmosphere and show little hysteresis, whereas old, deep ocean
608 water masses' responses to declining atmospheric CO₂ will be delayed, and thus show considerable
609 hysteresis. Over land, both the vegetation and soil carbon pools show a lagged response to decreasing
610 CO₂ due to the fact that transient changes in [CO₂] lead to a long term disequilibrium between the CO₂
611 fertilization effect, vegetation biomass, litterfall, and soil carbon (e.g., Krause et al. 2020). Therefore,
612 despite declining [CO₂] levels at the beginning of the ramp-down phase there is still an increase in
613 vegetation biomass due to CO₂ fertilization, and consequently an increase in soil carbon due to still
614 increasing litterfall. Warming-induced hysteresis appears to be larger for soil carbon in most models.
615 Similar to the large warming induced hysteresis (e.g., Schwinger and Tjiputra 2018; Schwinger et al.
616 2022; Santana-Falcón et al. 2023) in the ocean, this is caused by the fact that even though warming
617 levels start to decline shortly after the onset of the ramp-down phase, environmental conditions remain
618 warmer than in the pre-industrial period over the whole time of the ramp-down simulation.

619

620 3.3 Carbon cycle feedback metrics

621 3.3.1 Model mean global land and ocean responses

622 We now discuss the model-mean time evolution of the feedback metrics β and γ (Eqs. 1 and 2) derived
623 from the 1pctCO₂-cdr and ssp534-over simulations. In the ssp534-over scenario (Fig. 5a) the model-
624 mean feedback metric β_L increases monotonically from about 0.7 to 1.9 PgC ppm⁻¹ during the period
625 2000-2100. Over the ocean, β_O in the ssp534-over scenario decreases slightly until the mid-21st
626 century, and then it rises to about 1.7 PgC ppm⁻¹. Due to the much larger spread in carbon fluxes over
627 land (Fig. 2), the resulting model spread for both β_L and γ_L is also much larger than for β_O and γ_O .

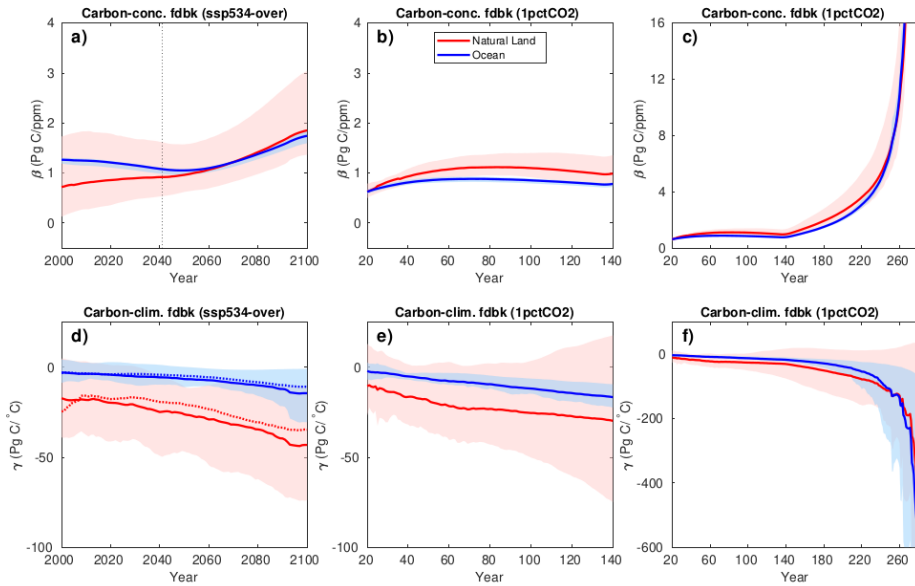
628 For the 1pctCO₂-cdr simulation, during the ramp-up phase over both land and ocean (Fig. 5b), β initially
629 increases and then decreases slightly with increasing [CO₂] consistent with the results of Arora et al.
630 (2013) for the same experiment but using CMIP5 ESMs. In contrast, during the ramp-down phase of the
631 1pctCO₂-cdr experiment, β reaches very high values over both land and ocean (Fig. 5c). This is because,
632 during the carbon removal phase of the 1pctCO₂-cdr experiment, there is a much larger amount of
633 accumulated ocean and terrestrial carbon for the same atmospheric CO₂ concentration due to the large
634 hysteresis seen in Figs. 3 and 4. Eventually, while [CO₂] is approaching pre-industrial values (i.e., $\Delta[\text{CO}_2]$
635 reaches zero), changes in cumulative fluxes (i.e., carbon stocks) relative to their pre-industrial values
636 remain positive, making β ill-defined towards the end of the 1pctCO₂-cdr ramp-down. For the same

Deleted: SSP5-3.4-05

Deleted: SSP5-3.4-05

Deleted: SSP5-3.4-05

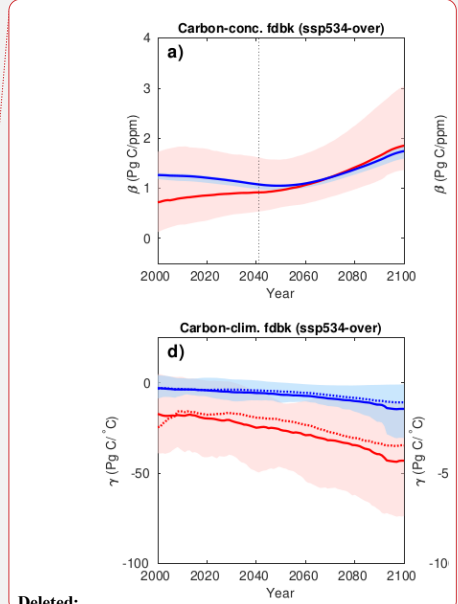
640 reason, an increase of β_L and β_O is also seen in the [ssp534-over](#) scenario after the CO₂ concentration
 641 peak in 2062.



642
 643 **Figure 5:** Model-mean β (a-c) and γ (d-f) feedback metrics in the [ssp534-over](#) and [1pctCO₂-cdr](#)
 644 experiments for natural land and ocean. Panels [b](#) and [e](#) show a zoom into the ramp-up phase of the
 645 time series shown on panels [c](#) and [f](#). Shadings show the range across the models. The dotted vertical
 646 line on panel [a](#) indicates where [CO₂] growth rate peaks in the fully coupled [ssp534-over](#) experiment.
 647 Dotted curves on panel [d](#) indicate the model mean with the assumption of negligible temperature
 648 change in the BGC simulation, (Eq. 2). An 11-year moving average has been used in all panels.

650 The model mean feedback factor γ is negative as the impact of climate change generally reduces the
 651 carbon stocks of land and ocean. In both [ssp534-over](#) and [1pctCO₂-cdr](#) experiments, the carbon-climate
 652 feedback is increasing over time (more negative γ , Fig. 5d and e), similar to figure 6 of Arora et al.
 653 (2013). The carbon-climate feedback is generally much smaller for the ocean than for land, and the
 654 model uncertainty for γ_O is only a small fraction of γ_L . Note that the same globally averaged surface air
 655 temperature anomaly is being used for the calculation of both γ_O and γ_L (Eq. 2). As noted above, the
 656 CanESM5 model simulates a globally increasing land uptake due to climate change towards the end of
 657 the [1pctCO₂-cdr](#) simulation (Fig. 4e), resulting in a positive γ_L for this model. During the ramp-down
 658 phase of the [1pctCO₂-cdr](#) experiment (Fig. 5f), γ reaches very large negative values. Similar to β , this is
 659 caused by the large hysteresis of the climate change impact on cumulative carbon stock while the
 660 surface temperature change becomes small (see Eq. 2). The assumption of $\Delta T^{BGC} = 0$ generally works

Deleted: SSP5-3.4-OS



Deleted:

Deleted: SSP5-3.4-OS

Deleted: (

Deleted:)

Deleted: (

Deleted:)

Deleted: SSP5-3.4-OS

Deleted: .

Deleted: SSP5-3.4-OS

671 well except for γ_L in the [ssp534-over](#) scenario where non-CO₂ forcings have a significant contribution
672 to ΔT^{BGC} (dashed curves in Fig. 5d).

Deleted: SSP5-3.4-O5

673 The global feedback factors B and Γ for the [ssp534-over](#) and 1pctCO₂-cdr simulations are shown in Fig.
674 S4. This feedback metric directly reflects the instantaneous fluxes, not cumulative fluxes, and is
675 therefore less influenced by the history of carbon fluxes, unlike β and γ . Consistent with Fig. 2, the
676 model-mean B remains positive during the [ssp534-over](#) simulation and during the positive emission
677 phase of the 1pctCO₂-cdr both over natural land and ocean. Only one model indicates a negative
678 carbon-concentration feedback over natural land towards the very end of the [ssp534-over](#) simulation
679 during its relatively short negative emission phase. B reflects the saturation of carbon sinks in the
680 1pctCO₂-cdr simulation with time and decreases monotonically during the positive emission phase.
681 Similar to what we have seen earlier for β , B shows large but negative values towards the end of the
682 1pctCO₂-cdr ramp-down phase (Fig. S4c).

Deleted: SSP5-3.4-O5

Deleted: SSP5-3.4-O5

Deleted: SSP5-3.4-O5

683 An interesting difference between the γ and Γ feedback metrics is seen towards the end of the 1pctCO₂-
684 cdr negative emissions phase (Fig. S4f), where Γ_L turns positive around year 180. This indicates that the
685 land biosphere starts gaining carbon that was previously lost due to the impacts of climate change. In
686 contrast, Γ_O remains negative indicating that the ocean continues to lose carbon due to warmer than
687 pre-industrial conditions until the end of the 1pctCO₂-cdr ramp-down phase. Because they are based
688 on cumulative emissions, both γ_O and γ_L remain negative throughout the 1pctCO₂-cdr ramp-down. This
689 illustrates that the use of a feedback metric based on time-integrated carbon fluxes might obscure
690 changes in important processes during net-negative emission phases. Eventually, both approaches for
691 calculating feedback metrics become ill-defined when the deviation of [CO₂] or temperature from their
692 pre-industrial values becomes small. This implies that both feedback metrics are not suited to describe
693 feedbacks towards the end (and beginning) of a concentration driven simulation set-up where pre-
694 industrial concentrations are restored. We note that this problem is connected to the choice of the
695 reference relative to which the feedbacks are calculated. In the approach of Chimuka et al. (2023),
696 where the reference is chosen to be at the transition from positive to negative emissions, singularities
697 towards the end of the 1pctCO₂-cdr simulation are avoided.

699 3.3.2 Model uncertainties and relative feedback strength in global feedback metrics

700 Figure 6 shows the model spread of feedback metrics at different points in time for the 1pctCO₂-cdr
701 simulation and the [ssp534-over](#) scenario (see also Table 2). The larger model-mean values during the
702 negative emission phases have been discussed in the previous section, but Fig. 6 also shows a strong
703 increase in model uncertainty (measured as the standard deviation around the model mean, Table 2)
704 between the ramp-up and ramp-down phase of the 1pctCO₂-cdr simulation. For both β_L and β_O , there
705 is either no (β_O) or only a small (β_L) increase in model uncertainty between the years 70 and 140 of the
706 1pctCO₂-cdr simulation, whereas at year 210 uncertainty has increased by about a factor of four. This
707 “jump” in uncertainty in β is solely caused by differences in how the models react to the sharp change
708 in forcing from increasing to decreasing CO₂ at year 140 (see Eq. 1, note that atmospheric CO₂ is
709 prescribed and ΔT^{BGC} is small). A similar behavior is seen for γ_O , while for γ_L the increase in model

Deleted: SSP5-3.4-O5

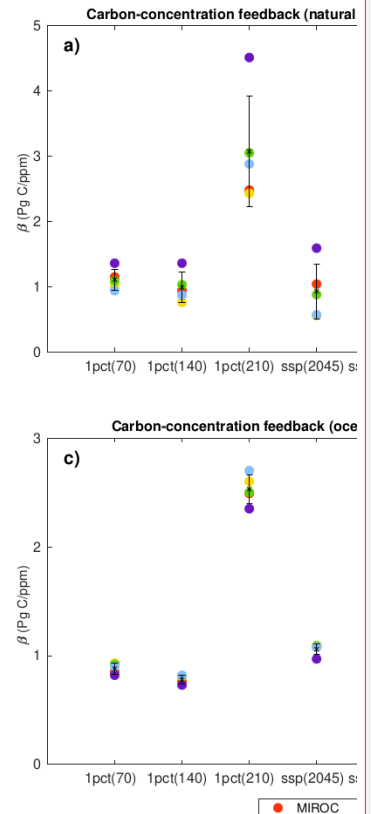
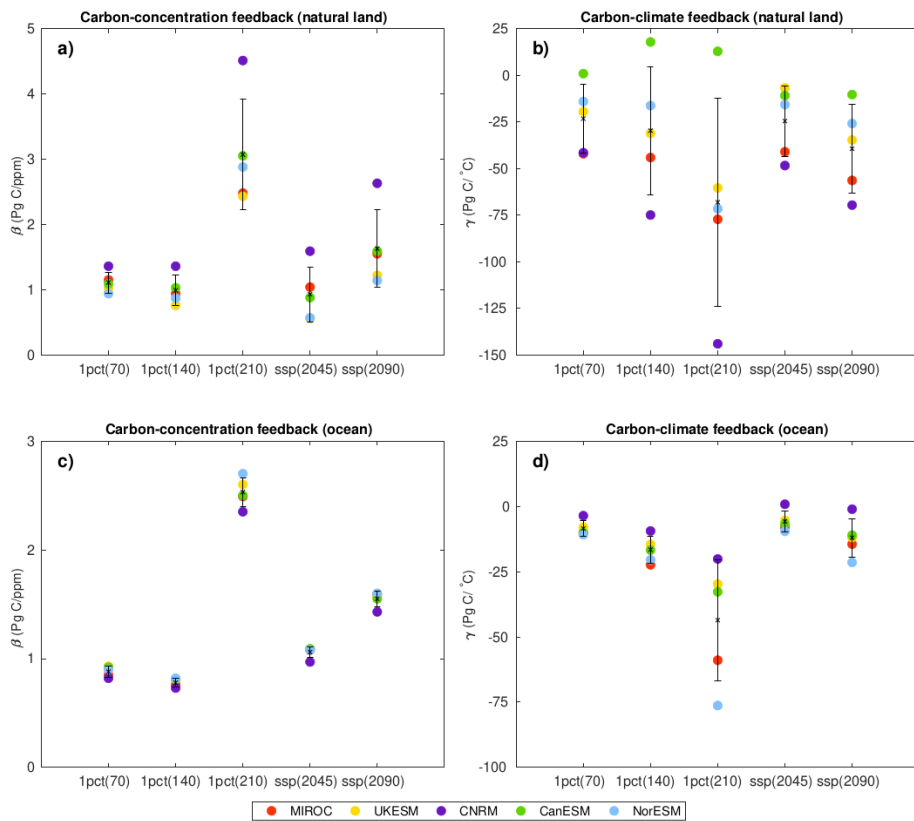
715 uncertainty is more gradual, i.e., the increase between years 70 and 140 is about the same as between
716 years 140 and 210. There is also a consistent increase in model uncertainty in all feedback metrics from
717 the positive to the negative emissions phase in the [ssp534-over](#) scenario.

Deleted: SSP5-3.4-05

718 The relative strength of the feedback among the models remains relatively stable over time, between
719 positive and negative emission phases, and between the different experiments. Model A having a
720 stronger (weaker) feedback than model B at one of the instances depicted in Fig. 6, indicates that model
721 A will have a stronger (weaker) feedback than model B for the other instances with only few exceptions.
722 Most of these exceptions arise because modeled feedbacks are very similar such that small changes in
723 feedback strength can lead to a different ranking. In a few cases relative feedback strength evolves
724 differently in the models. For example, NorESM2-LM evolves from having a weaker than average γ_L in
725 the positive emission phase of the [1pctCO₂-cdr](#) simulation to having a stronger than average γ_L in the
726 negative emission phase.

727 Finally, it is worth noting that while the model uncertainty in γ_O is much smaller than in γ_L during the
728 ramp-up phase of the [1pctCO₂-cdr](#) simulation (uncertainty in γ_O is only 15% of those in γ_L at year 140),
729 this situation has changed for the ramp-down phase. At year 210, the uncertainty in the ocean carbon-
730 climate feedbacks has grown much stronger than the uncertainties of the terrestrial carbon-climate
731 feedback, such that model uncertainties in γ_O are 42% of those in γ_L .

732



Deleted:

Deleted: feedback metrics

Deleted: SSP5-3.4-OS

Deleted: feedback metrics

Deleted: at the ramp-up and ramp-down phases

Deleted: SSP5-3.4-OS

Figure 6: Globally averaged values of β (a and c) and γ (b and d) in the 1pctCO₂-cdr (years 70, 140, and 210) and ssp534-over (years 2045 and 2090) experiments for natural land and ocean. The bars show the mean \pm 1 standard deviation range, and the individual colored dots represent individual models.

Table 2: Globally averaged values of β (Pg C ppm⁻¹) and γ (Pg C °C⁻¹) at years 70, 140, and 210 of the 1pctCO₂-cdr simulation and years 2045 and 2090 of the ssp534-over experiment for natural land and ocean.

	MIROC-ES2L	UKESM1-0-LL	CNRM-ESM2-1	CanESM5	NorESM2-LM	Mean
$\beta_{L(70)}$	1.15	1.02	1.36	1.09	0.94	1.11 (SD=0.16)
$\beta_{L(140)}$	0.94	0.76	1.36	1.03	0.87	0.99 (SD=0.23)

$\beta_{L(210)}$	2.48	2.43	4.51	3.05	2.88	3.07 (SD=0.85)
$\beta_{L(2045)}$	1.04	0.56	1.59	0.88	0.57	0.93 (SD=0.42)
$\beta_{L(2090)}$	1.55	1.22	2.63	1.59	1.14	1.63 (SD=0.59)
$\gamma_{L(70)}$	-42.14	-19.54	-41.58	0.82	-14.12	-23.31 (SD=18.5)
$\gamma_{L(140)}$	-44.17	-31.19	-74.97	17.78	-16.31	-29.77 (SD=34.3)
$\gamma_{L(210)}$	-77.26	-60.45	-144.01	12.77	-71.64	-68.12 (SD=55.8)
$\gamma_{L(2045)}$	-41.08	-6.80	-48.46	-10.93	-15.78	-24.61 (SD=18.9)
$\gamma_{L(2090)}$	-56.43	-34.76	-69.66	-10.41	-25.95	-39.44 (SD=23.7)
$\beta_{O(70)}$	0.85	0.93	0.82	0.92	0.90	0.88 (SD=0.05)
$\beta_{O(140)}$	0.76	0.81	0.73	0.81	0.82	0.78 (SD=0.04)
$\beta_{O(210)}$	2.49	2.60	2.35	2.50	2.70	2.53 (SD=0.13)
$\beta_{O(2045)}$	1.08	1.09	0.97	1.09	1.08	1.06 (SD=0.05)
$\beta_{O(2090)}$	1.59	1.57	1.43	1.55	1.60	1.55 (SD=0.07)
$\gamma_{O(70)}$	-10.09	-7.95	-3.60	-10.13	-10.84	-8.52 (SD=2.96)
$\gamma_{O(140)}$	-22.40	-14.56	-9.44	-16.77	-20.48	-16.61 (SD=5.10)
$\gamma_{O(210)}$	-58.94	-29.78	-20.16	-32.75	-76.28	-43.59 (SD=23.2)
$\gamma_{O(2045)}$	-7.88	-5.43	0.78	-6.75	-9.56	-5.77 (SD=3.96)
$\gamma_{O(2090)}$	-14.50	-11.98	-1.10	-11.05	-21.50	-12.03 (SD=7.35)

Deleted: γ_L

Deleted: γ_L

Deleted: γ_L

Deleted: γ_L

Deleted: γ_L

Deleted: γ_O

Deleted: γ_O

Deleted: γ_O

Deleted: γ_O

Deleted: γ_O

749

750

751

3.3.3 Model differences in the terrestrial carbon-concentration feedback

752 Figure 7 shows the individual components of the decomposition of β (Eq. 4), separately for tropical and
 753 subtropical (30°S-30°N) and higher latitudes (between 30°N/S and the poles), both on the ramp-up and
 754 ramp-down phases (years 70 and 210, respectively) of the 1pctCO₂-cdr-bgc experiment. The time
 755 periods are selected such that the atmospheric CO₂ concentration is the same (569 ppm, a doubling of
 756 pre-industrial CO₂ concentration). All models consistently show increases in both $\tau_{cveg\Delta}$ and $\tau_{csoil\Delta}$
 757 during the ramp-down compared to the ramp-up phase, since these metrics are based on cumulative

Deleted: 3

769 vegetation and soil carbon (Eq. 4), which are slower than NPP and GPP in reacting to decreasing [CO₂].
 770 Lower (higher) latitudes are associated with higher $\tau_{cveg\Delta}$ ($\tau_{csoil\Delta}$). Likewise, the litterfall term $\frac{\Delta LF}{[CO_2]}$ is
 771 larger during the ramp-down phase in all models due to lagged reaction of vegetation carbon to the
 772 decrease in [CO₂], with this effect being generally most pronounced at low latitudes. There is also a
 773 consistent but small increase in the term $\frac{\Delta GPP}{[CO_2]}$, which represents the CO₂ fertilization effect. This
 774 increase implicitly includes the effect of changes (typically an increase) in standing vegetation biomass
 775 and leaf area index for all models but also changes in vegetation cover as [CO₂] varies for UKESM1-0-LL
 776 that simulates dynamic vegetation cover. For the dimensionless fractions $\frac{\Delta R_h}{\Delta LF}$ and CUE_Δ, changes
 777 between ramp-up and ramp-down phases are less consistent between the models. For CUE_Δ, three
 778 models show an increase and two models a decrease, although the changes between ramp-up and
 779 ramp-down phases are generally small. For $\frac{\Delta R_h}{\Delta LF}$ changes range from a 115% increase (CNRM-ESM2-1
 780 at low latitudes) to a small decrease (UKESM1-0-LL). It is worth noting that for four out of six terms of
 781 Eq. 4 ($\tau_{cveg\Delta}$, $\tau_{csoil\Delta}$, $\frac{\Delta R_h}{\Delta LF}$, and $\frac{\Delta LF}{[CO_2]}$) the model disagreement is significantly larger during the ramp-
 782 down phase of the 1pctCO₂-cdt simulation, indicating that changes in these processes are responsible
 783 for the strong increase in model uncertainty in β_L between positive and negative emission phases
 784 pointed out in the previous section.

785 The decomposition applied here helps to understand some of the model differences visible in Fig. 4. As
 786 already pointed out in Arora et al. (2020), the high accumulation of terrestrial carbon by the CNRM-
 787 ESM2-1 model in the BGC simulation (Fig. 4b) is not caused by a particularly strong CO₂ fertilization
 788 effect or CUE_Δ but rather by relatively high values of $\tau_{cveg\Delta}$ and $\tau_{csoil\Delta}$, indicating long residence
 789 timescales in vegetation and soil. Likewise, CanESM5's higher than average atmosphere-land C flux (Fig.
 790 4b), despite its near-average strength of the CO₂ fertilization effect and soil and vegetation turnover
 791 times is due to its high CO₂ fertilization effect at lower latitudes and also its high CUE_Δ through which
 792 the model converts a much larger fraction of GPP to NPP. Compared to the other models, CanESM5
 793 also shows the largest relative increase (85% and 134% for lower and higher latitudes, respectively) in
 794 $\tau_{csoil\Delta}$ between years 70 and 210.

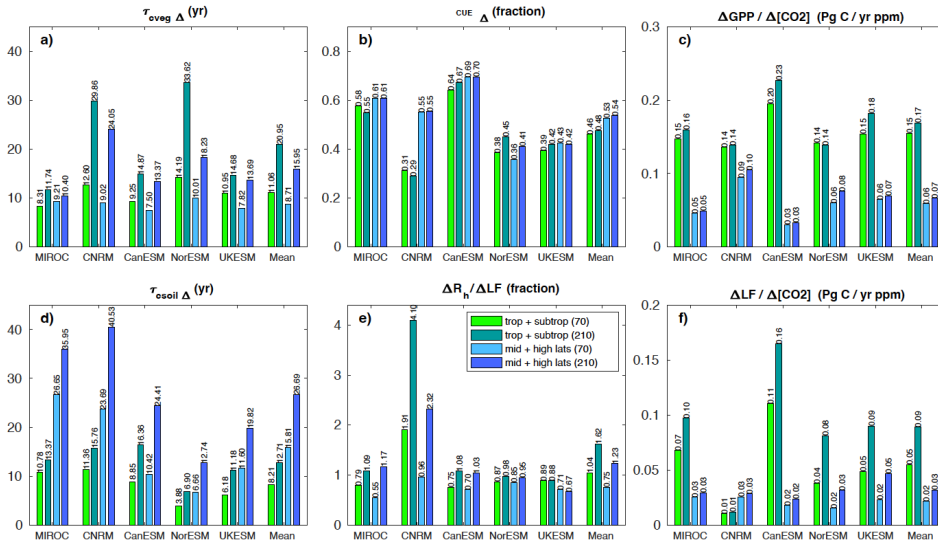
795
 796

Deleted: 3

Deleted: UKESM

Deleted: UKESM

Deleted: 3

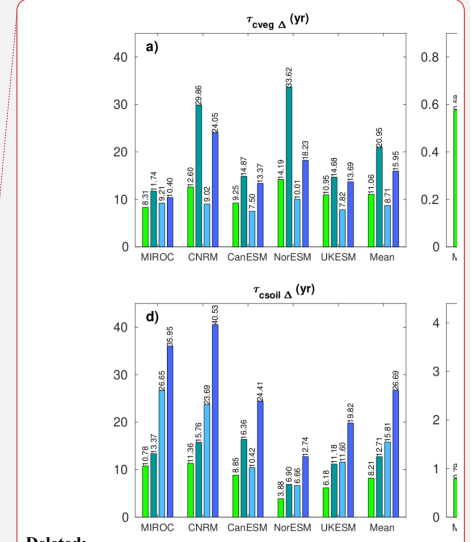


801 **Figure 7:** Individual terms of Eq. (4) contributing to β_L . Values for tropical and subtropical (between
 802 30°S and 30°N) regions are in green, and for northern and southern latitudes (above 30°S and 30°N) are
 803 in blue. Lighter (darker) color on each panel corresponds to the middle of the ramp-up (ramp-down)
 804 phase of the 1pctCO₂-cdr-bgc experiment (years 70 and 210, respectively).
 805
 806
 807

808 3.3.4 Northern hemisphere high-latitude permafrost and non-permafrost regions

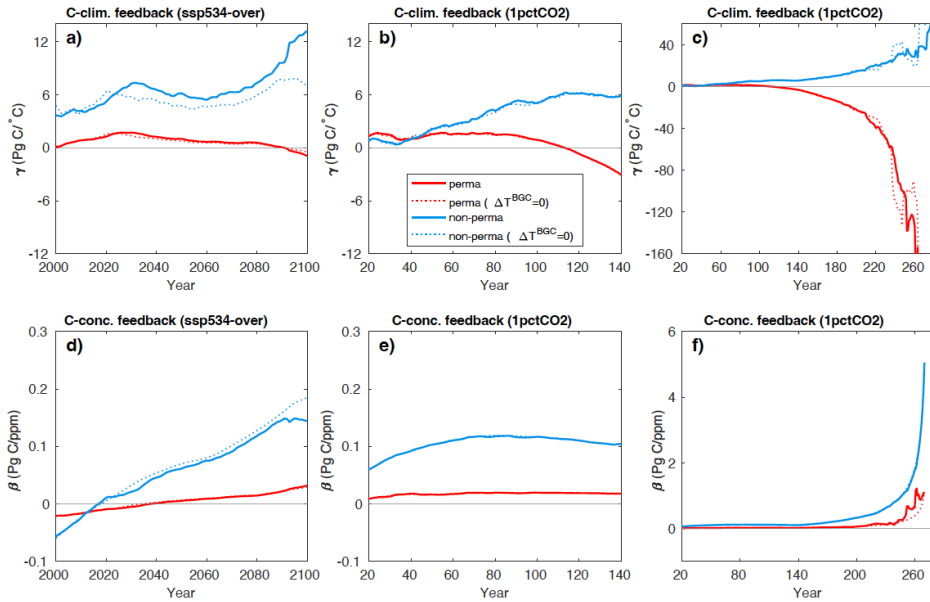
809 Of the ESMs considered here, only NorESM2-LM has a terrestrial model that vertically resolves soil
 810 carbon (CLM5, Lawrence et al. 2019). Since this is a prerequisite to skillfully simulate carbon release
 811 during gradual permafrost degradation, we restrict our analysis of high latitude and permafrost
 812 feedbacks to the NorESM2-LM model. If only natural land is considered, the area associated with
 813 permafrost and non-permafrost regions north of 45°N is about 14.7 and 17.5 x10⁶ km², respectively
 814 (total area is 14.7 and 24.1 x10⁶ km²).

815 The effect of warming on carbon uptake in the high-latitude non-permafrost region is positive ($\gamma > 0$,
 816 increased uptake) in NorESM2-LM in both the ssp534-over and the 1pctCO₂-cdr simulation (Fig. 8a-c,
 817 blue lines). Within the permafrost region, γ is close to zero for the ssp534-over simulation up to 2100
 818 and the ramp-up phase of the 1pctCO₂-cdr simulation (Fig. 8a,b, red line), albeit with a decreasing (more
 819 negative) trend. This is due to a compensation of vegetation carbon gain and soil carbon losses (Fig.
 820 S5). During the ramp-down phase of the 1pctCO₂-cdr simulation, permafrost soil carbon losses increase
 821 approximately until year 210 of the simulation (Fig. S5). Thereafter, permafrost soil carbon stays roughly
 822 constant with a cumulative loss of about 55 PgC over the simulation. Vegetation carbon over the
 823 permafrost region still increases for the first 30 years of the ramp-down phase of the 1pctCO₂-cdr



- Deleted:
- Deleted: 3
- Deleted: bgc and 1pctCO2-
- Deleted: experiments
- Deleted: models
- Deleted: SSP5-3.4-0S
- Deleted: SSP5-3.4-0S

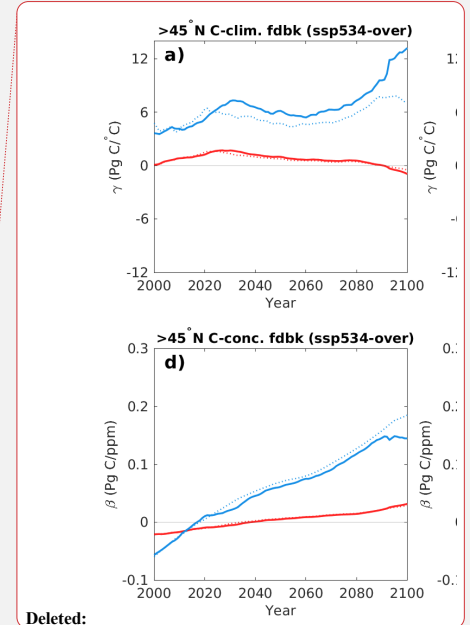
831 simulation, after which it decreases mainly due to decreasing temperature (Fig. S5g). The γ value
 832 calculated for the permafrost region, therefore, shows a sharp decrease during the ramp-down period
 833 of the 1pctCO₂-cdr simulation (Fig. 8c). Eventually, when ΔT approaches small values γ loses its
 834 significance as seen before for the global feedback factors.



835
 836 **Figure 8:** γ (a-c) and β (d-f) for northern hemisphere high latitude (above 45°N) natural land permafrost
 837 and non-permafrost regions in the ssp534-over and 1pctCO₂-cdr simulations using the NorESM2-LM
 838 model. An 11-year moving average has been used in all panels.

840 In both the ssp534-over scenario and the 1pctCO₂-cdr simulations, β is positive (except initially in the
 841 ssp534-over simulation) although the absolute values remain very small. The carbon-concentration
 842 feedback is stronger over the non-permafrost area, where both soil and vegetation carbon increase
 843 than over the permafrost area, where soil and vegetation carbon stay almost constant in the BGC
 844 simulation (Fig. S5).

845 NorESM2-LM has the smallest transient climate response (TCR) of the models considered here, and it
 846 can be expected that the permafrost carbon-climate feedback estimated here would be larger in a
 847 model with higher TCR. Nevertheless, the permafrost carbon loss of 26.9 Pg C °C⁻¹ in the year 210 of the
 848 simulation contributes 38% of the total carbon-climate feedback at this point in time in NorESM2-LM.



Deleted:
 Deleted: SSP5-3.4-O5
 Deleted: NorESM
 Deleted: SSP5-3.4-O5
 Deleted: SSP5-3.4-O5
 Deleted: in the BGC simulation
 Deleted: NorESM2

849

857 **3.4 Geographical pattern of carbon cycle feedback metrics**

858 We have calculated β and γ feedback factors at grid-scale to assess the spatial patterns of feedbacks
859 over the land and ocean (Figs. 9 and 10). In order to compare positive and negative emission phases,
860 we selected 21-year time intervals centered at years 70 and 210 of the ramp-up and ramp-down phases
861 of the 1pctCO₂-cdr simulation, at an atmospheric CO₂ concentration of 570 ppm (corresponding to a
862 doubling of pre-industrial CO₂ concentration). We also selected a 21-year time-interval centered at year
863 2045 (corresponding to CO₂ concentration of 523 ppm), shortly before the CO₂ peak of the ssp534-over
864 scenario. We have also analyzed a 21-year time interval during the net-negative emission phase of the
865 SSP scenario (centered at year 2090), but since the time-period of net-negative emissions in the SSP-
866 scenario is relatively short, we focus on comparing the feedbacks during the positive and negative
867 emission phases of the 1pctCO₂-cdr simulation alongside with the feedbacks during the positive
868 emission phase of ssp534-over. For completeness, Fig. S6 shows the spatially resolved feedback during
869 the net-negative emission phase of ssp534-over.

Deleted: SSP5-3.4-O5

Deleted: SSP5-3.4-O5

Deleted: SSP5-3.4-O5

870 In the 1pctCO₂-cdr simulation, rising [CO₂] increases the modeled carbon sinks almost everywhere (i.e.,
871 positive β) over the land and ocean (Fig. 9a-e). CanESM5 shows a weak negative β over northern high-
872 latitude land areas, and there are some spurious negative values of β over desert areas in some models.
873 For the ocean, all models agree that the regions with the strongest increase of the oceanic CO₂ sinks in
874 response to higher [CO₂] are the North Atlantic and the Southern Ocean. As seen for the global average
875 (Fig. 5), β remains positive and increases in magnitude during the ramp-down phase (Fig. 9 f-j, note the
876 different color scale). As an overarching observation, the large scale patterns of the carbon-
877 concentration feedback are remarkably similar during the ramp-up and ramp-down phases of the
878 1pctCO₂-cdr simulation (with spatial correlations, averaged across all the models, of 0.93 and 0.80 over
879 land and the ocean, respectively) but the magnitude of the feedback is about two times larger in the
880 ramp-down phase, consistent with the lagged response of cumulative carbon uptake to the decrease
881 in atmospheric CO₂ (Figs. 3 and 4). The most prominent change in the spatial pattern of β occurs in
882 the equatorial Pacific. All models consistently show that this area has turned from a cumulative carbon
883 sink at year 70 to a cumulative carbon source at year 210.

884 We find the largest values of β over tropical land and to a lesser extent over northern hemisphere
885 temperate and boreal ecosystems coincident with areas of large biomass (forests). For three of the
886 models (NorESM2-LM, CanESM5, and UKESM1-0-LL), the feedback is clearly dominated by tropical and
887 subtropical regions, while for MIROC-ES2L the feedback is approximately of the same strength in
888 northern temperate and high-latitude regions. For CNRM-ESM2-1, the carbon-concentration feedback
889 is on average stronger north of 30° latitude than in tropical/subtropical regions. For NorESM2-LM and
890 UKESM1-0-LL, the tropical dominance of the carbon-concentration feedback stems from vegetation
891 carbon, while for CanESM5 both vegetation and soil carbon contribute about equally (Figs. S7 and S8).

892 The results presented in Section 3.3.3 provide to some extent a mechanistic understanding of these
893 model differences. CNRM-ESM2-1 has the highest CO₂ fertilization effect $\frac{\Delta GPP}{[CO_2]}$ in high latitudes and

897 the lowest $CUE\Delta$ at low latitudes. This, combined with a large high-latitude $\tau_{csoil\Delta}$ leads to a larger
898 carbon accumulation in vegetation and soil in higher latitudes than in the tropics/subtropics in this
899 model. The three models with tropical dominance of β (NorESM2-LM, CanESM5, and UKESM1-0-LL)
900 have a relatively high $\tau_{cveg\Delta}$ and relatively low $\tau_{csoil\Delta}$. CanESM5, shows the strongest
901 tropical/subtropical CO_2 fertilization effect, but also a large response of the litterfall term leading to
902 large responses in both vegetation and soil carbon.

903 In the ssp534-over simulation, the ocean β magnitude is similar to that of the 1pct CO_2 -cdr simulation
904 and the spatial distribution of the ocean response to the $[CO_2]$ rise is roughly consistent between the
905 models (Fig. 9k-o). In contrast, the feedback pattern over natural land is different in some regions and
906 models between the SSP scenario simulation and the idealized 1pct CO_2 -cdr experiment. UKESM1-0-LL,
907 CanESM5, and to a lesser extent NorESM2-LM project negative β values in some northern high latitude
908 regions (e.g., Siberia). These negative β values are either not seen at all (UKESM1-0-LL, NorESM2-LM)
909 or are weaker (CanESM5) in the 1pct CO_2 -cdr simulation, and they originate from a combination of
910 vegetation and soil carbon pools (Figs. S7 and S8). Unlike in the 1pct CO_2 -cdr experiment, temperature
911 changes are not negligible in the BGC simulation of the ssp534-over experiment (Fig. 1). Furthermore,
912 the spatial pattern of temperature changes is very different for some models, particularly for UKESM1-
913 0-LL, NorESM2-LM, and CNRM-ESM2-1, which show local cooling that is not present (or much weaker)
914 in the fully coupled simulations (Fig. S9). This cooling (and other changes in surface climate related to
915 non- CO_2 forcings) lead to local carbon losses and negative β -values in UKESM1-0-LL and NorESM2-LM
916 in northern high latitudes. In addition, according to Eq. 3, these negative values are reinforced by
917 positive γ -values in this region and a positive global mean temperature change in ssp534-over in these
918 models (see Eq. 3). In contrast, CNRM-ESM2-1 does not show negative values of β in northern high
919 latitudes (despite local cooling), which can be explained by much larger β -values to begin with, and a
920 smaller (and negative) temperature sensitivity γ in high latitudes.

Deleted: SSP5-3.4-05

Deleted: SSP5-3.4-05

Deleted: Nevertheless

Deleted: distribution of the feedback factor β calculated with the assumption $\Delta T^{BGC} = 0$ results in a similar

Deleted: (not shown), which suggests that the non-negligible

Deleted: in the BGC simulation are not the cause

Deleted: these negative values of β . Rather

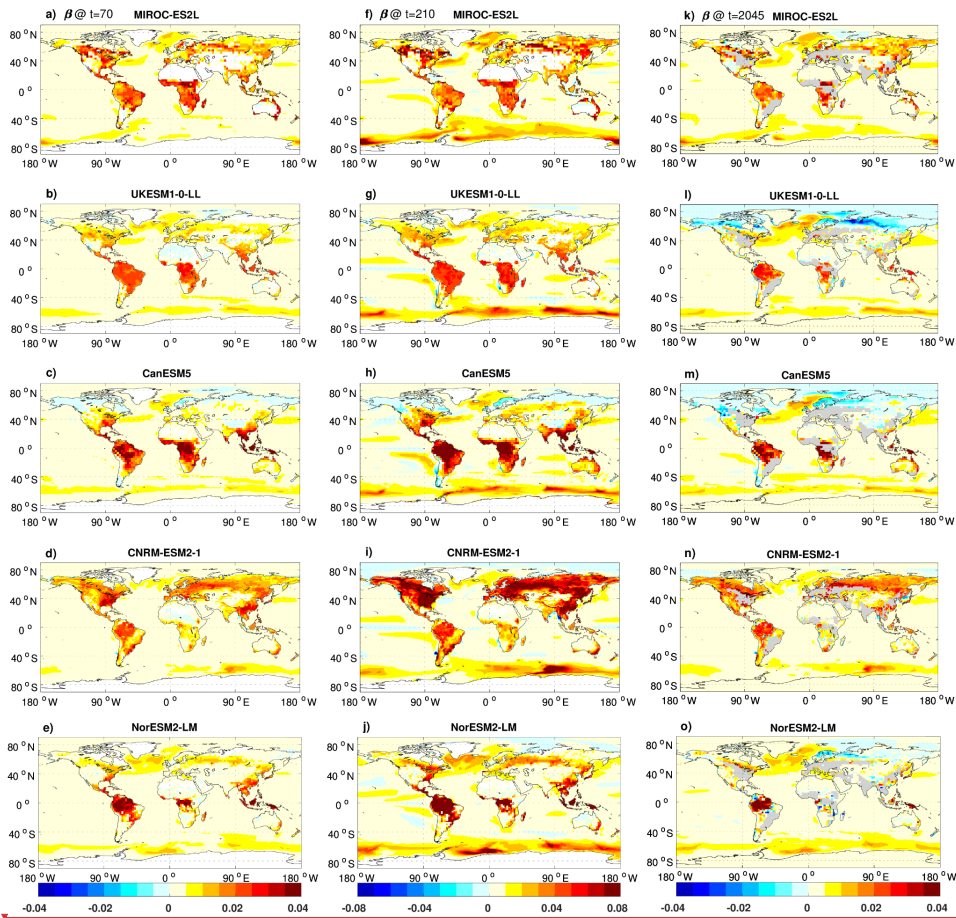
Deleted: most likely caused

Deleted: remaining land use

Deleted: grid cells that we have classified as "natural" land with our simple threshold approach. This is consistent with the fact that the high-latitude negative β values occur in those models that have low β in these regions in the 1% simulation (i.e., a relatively small land use change perturbation...

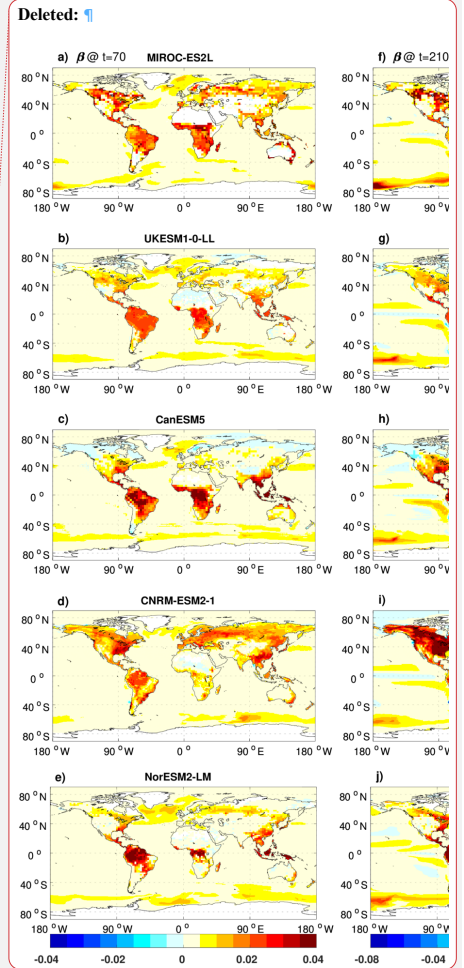
Deleted: change β from positive to

Deleted:).



941 **Figure 9:** The spatial distribution of β ($\text{kg C m}^{-2} \text{ppm}^{-1}$) at year 70 of the ramp-up phase of the 1pctCO₂-
 942 cdr simulation (a-e), at year 210 of the ramp-down phase of the 1pctCO₂-cdr simulation (f-j), and at year
 944 2045 (natural land only, gray areas are crop-dominated grid cells) during the positive emission phase of
 945 the sps534-over scenario (k-o).

946
 947
 948 Figure 10 indicates that the ESMs considered here simulate predominantly negative values of γ_0 over
 949 the ocean. Positive values of γ_0 are found in the Arctic, and in the Southern Ocean most models
 950 simulate a banded pattern of positive (adjacent to Antarctica), negative (centered between 60 and
 951 50°S), and positive (between approximately 50 and 40°S) values. In the region adjacent to Antarctica,
 952 climate change increases the ocean CO₂ sink, mainly due to a reduction in sea ice coverage (Roy et al.



- Deleted: white
- Deleted: SSP5-3.4-OS
- Deleted: some cases in parts of
- Deleted: polar
- Deleted: . Climate
- Deleted: in these regions

961 2011; Schwinger et al. 2014). The North Atlantic Ocean and the Southern Ocean have the largest
962 negative γ_o values due to changes in ocean circulation and deep water formation. In tropical and
963 subtropical ocean regions, the reduced oceanic carbon uptakes can be attributed to warming-induced
964 decreased CO₂ solubility and increased stratification (Roy et al. 2011).

965 Over land, climate change generally reduces carbon sinks in the tropics and mid-latitudes. In the high
966 latitudes models disagree on the strength and the sign of the carbon-climate feedback. CNRM-ESM2-1
967 shows relatively strong soil carbon losses in northern high latitudes, which overcome vegetation carbon
968 gains (Figs. S10 and S11) leading to mostly negative values of γ_L in this region. As mentioned above,
969 CanESM5's carbon-climate feedback switches from weakly negative at 2xCO₂ to positive at 4xCO₂.
970 Figure 10c clearly shows that the positive global γ values originate from the northern hemisphere high
971 latitudes. Also, the positive γ_L in CanESM5 over the northern high latitudes is seen in both vegetation
972 and soil carbon reservoirs, but with a time lag for soil carbon. Consistent with our analysis in Sect. 3.3.4,
973 NorESM2-LM shows permafrost carbon loss in north-eastern Siberia and northern Alaska, but these
974 losses become significant only during the ramp-down phase of the 1pctCO₂-cdr simulation (Fig. 10j).

975 The spatial pattern of the carbon-climate feedback is similar during the ramp-up and ramp-down phases
976 of the 1pctCO₂-cdr simulation, but the magnitude has roughly doubled during the ramp-down phase,
977 consistent with the cumulative nature of the γ feedback metric used here (note the different color-
978 scales in Fig. 10). The correlations of the spatial patterns (at years 70 and 210) are lower than for β and
979 range from 0.41 (MIROC-ES2L) to 0.66 (UKESM1-0-LL) for γ_o and from 0.49 (NorESM2-LM) to 0.88
980 (UKESM1-0-LL) for γ_L .

981 The value of the γ feedback metric in the ssp534-over scenario simulation is less affected by land-use
982 change, since the same land-use changes are imposed in both the COU and the BGC simulation. In
983 contrast to β , which is directly altered by carbon stock changes due to land-use changes, γ is only
984 influenced indirectly, possibly by different sensitivities of the new vegetation cover after a land-use
985 transition, or by changes in local to regional climatic conditions. In the global mean, the carbon-climate
986 feedback during the positive emission phase is very similar for the SSP scenario and the 1pctCO₂-cdr
987 simulation (Fig. 5d and e). Also, the spatial patterns of γ_L are largely similar between the ssp534-over
988 and the ramp-up phase of the 1pctCO₂-cdr simulation with correlations ranging from 0.71 (NorESM2-
989 LM) to 0.84 (CNRM-ESM2-1). The largest difference between the two simulations is an enhanced
990 positive feedback over northern high-latitude land in the UKESM1-0-LL model in the SSP scenario
991 compared to the 1pctCO₂-cdr simulation, which is seen in both vegetation and soil carbon pools (Figs.
992 S10 and S11). These differences are related to the negative β -values (discussed above) for these
993 models, which make the carbon gain due to warming (the difference $\Delta C^{cou} - \Delta C^{bgc}$) considerably
994 larger than in the 1pctCO₂ simulation. Again, this is reinforced by the fact that the global average
995 temperature change in the ssp534-over simulation is positive and thus ($\Delta T^{cou} - \Delta T^{bgc}$) is smaller than
996 the actual (local) temperature differences. This indicates that, if the global mean temperature change
997 due to non-CO₂ forcings does not broadly reflect local changes correctly (e.g., local cooling vs. global
998 warming), regional scale feedback factors might show unexpected results.

Deleted: Fig. S9

Deleted: S10

Deleted: weak

Deleted: 9c

Deleted: 9j

Deleted: 9

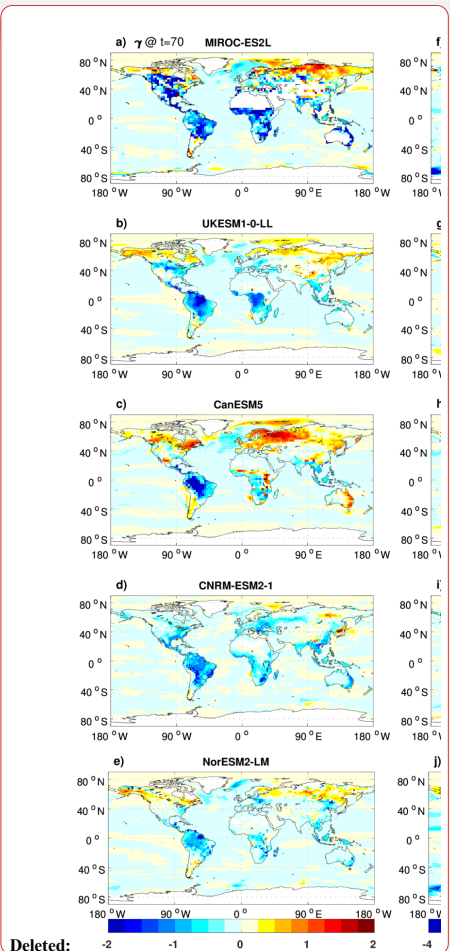
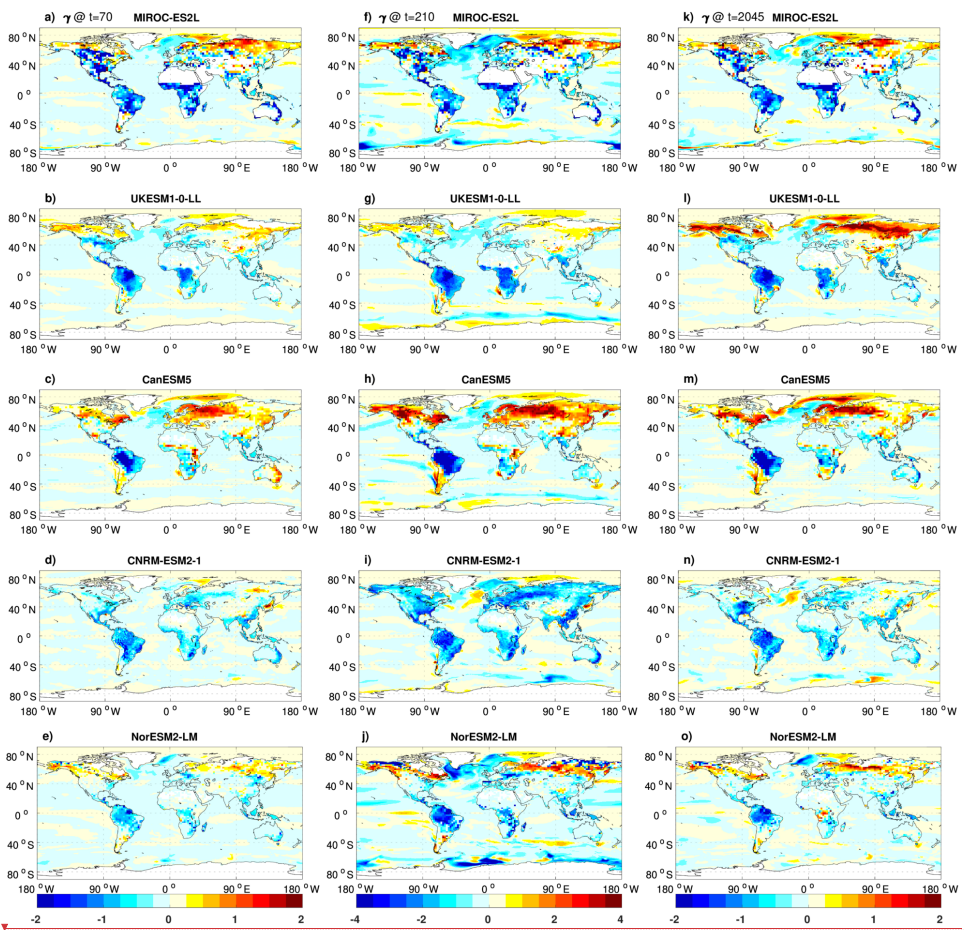
Deleted: SSP5-3.4-OS

Deleted: SSP5-3.4-OS

Deleted: SSP scenario compared to the 1pctCO₂ simulation, which is seen in both vegetation and soil carbon pools (Figs. S9 and S10). ...

1010 Over the ocean the global mean carbon-climate feedback is slightly smaller in ssp534-over compared
 1011 to the 1pctCO₂-cdr simulation (Fig. 3f), but again, the spatial pattern is largely similar with correlations
 1012 ranging from 0.47 (CNRM-ESM2-1) to 0.78 (MIROC-ES2L).
 1013

Deleted: SSP5-3.4-05



Deleted:

1014 **Figure 10:** same as Fig. 9 but for γ ($\text{kg C m}^{-2} \text{C}^{-1}$). Note that cropland areas are not excluded from panels
 1015 (k-o) as in Fig. 9.
 1016
 1017

1018 **4. Summary and conclusions**

1019 We have investigated carbon cycle feedbacks in a highly idealized model experiment with exponentially
 1020 increasing and decreasing atmospheric CO₂ concentration (1pctCO₂-cdr) and in a more realistic

overshoot scenario simulation ([ssp534-over](#)). We employ an ensemble of five CMIP6 ESMs that have run additional (biogeochemically coupled) simulations that allow us to separate the effects of changing atmospheric CO₂ and of changing surface climate on the simulated carbon cycle.

Deleted: SSP5-3.4-OS

We find that both the carbon-concentration (β) and the carbon-climate (γ) feedbacks show a considerable hysteresis behavior during negative emission phases. The well-known reduction of ocean and land carbon uptake with increasing temperatures continues long into the negative emissions phases of the simulations (when temperature is decreasing), albeit at a reduced rate. For the ocean, there is still a reduction in carbon stocks due to legacy warming when pre-industrial atmospheric CO₂ is restored in the 1pctCO₂-cdr simulation, consistent with the single-model studies of Schwinger and Tjiputra (2018) and Bertini and Tjiputra (2022). In contrast, all models agree that the effect of legacy warming is less important for the terrestrial carbon-climate feedback as the reduction of global mean surface temperature leads to a reduction in temperature-induced losses of terrestrial carbon towards the end of the 1pctCO₂-cdr simulation.

Deleted: We discuss global mean carbon fluxes and employ the widely used carbon cycle feedback metrics of β and γ (Friedlingstein et al. 2003) to compare feedbacks between models and between phases of (implied) positive and negative CO₂ emissions as well as the (model) uncertainty of these feedbacks. To determine the sources of uncertainty for the terrestrial carbon-concentration feedback, we also decompose β_L into contributions from different processes following the methodology of Arora et al. (2020), and investigate spatial feedback patterns and their changes.

Deleted: Hysteresis is stronger for the ocean relative to the strength of the feedbacks, although the hysteresis of the terrestrial carbon cycle feedbacks is larger in absolute terms.

Carbon cycle feedback metrics vary over time, and between different scenarios. When the deviations in surface temperature and atmospheric CO₂ become small towards the end of a modeled negative emission scenario, the magnitude of these feedback metrics “explodes” since they are defined as the ratio between the deviations in carbon stocks and the change in temperature and atmospheric CO₂, respectively. Arguably, the latter is mainly a problem due to the strongly idealized simulation design of the 1pctCO₂-cdr experiment, not for more realistic scenarios as the ssp534-over. Also, a different definition of the reference state for the feedback metrics, as proposed by Chimuka et al. (2023), avoids this problem.

Deleted: It is well known that carbon

Deleted: Here we find that when (implied) emissions change from positive to negative, β and γ (defined according to Friedlingstein et al. 2003) show an increase in absolute values due to the large hysteresis of carbon stock changes, while temperature and atmospheric CO₂ decrease. Particularly, if

Deleted: experiment, not for more realistic scenarios as the SSP5-3.4-OS. The feedback metrics B and Γ (defined according to Boer and Arora, 2009), which are based on instantaneous fluxes, also become ill-defined when deviations of surface temperature and atmospheric CO₂ approach zero, but unlike the β and γ feedback metrics, they are only indirectly affected by the history of carbon fluxes. These metrics thus respond faster to changes in atmospheric CO₂ concentration or temperature, for example, B clearly shows the point in time when carbon fluxes reverse and the land or ocean turn from a sink to a source of carbon under negative emissions

Deleted: SSP5-3.4-OS

We find that the relative strength of the feedback remains relatively robust between positive and negative emission phases and between the different simulations considered here. For example, a model with a stronger than average terrestrial carbon-concentration feedback (β_L) during the positive emission phase of the 1pctCO₂-cdr simulation will also show a stronger than average β_L during the negative emission phase or for the ssp534-over scenario. Regarding the model uncertainty of feedback metrics we find that there is an increase in uncertainty in all feedback metrics between the positive and negative emission phases of the 1pctCO₂-cdr simulation. Except for γ_L , this increase is much larger than expected from an accumulation of uncertainty over time. This indicates that there is an additional component of model uncertainty resulting from differences in the lagged model responses to the change from increasing to decreasing radiative forcing.

Deleted: uncertainties

The geographical patterns of terrestrial β and γ feedback metrics highlight differences in the responses of tropical/subtropical versus temperate/boreal ecosystems as a major source of model disagreement. For individual models, however, the spatial feedback patterns are remarkably similar during phases of increasing CO₂ compared to phases of decreasing CO₂ concentrations, indicating that the increase of global mean values of β and γ due to lagged responses of the carbon cycle during negative emissions phases does not stem from a particular region but is generally seen over the whole globe. We estimate the contribution of permafrost carbon release to the carbon-climate feedback only for one of the five ESMs (NorESM2-LM, which vertically resolves soil carbon). Permafrost carbon release is clearly seen as a strong positive feedback (i.e., negative γ) over the permafrost area, but it emerges only relatively late

Deleted: feedback

1099 in the simulations. Permafrost carbon release accounts for 38% of NorESM2-LM's carbon-climate
1100 feedback at the midpoint of the negative emission phase of the 1pctCO₂-cdr simulation.

1101 In the spp534-over simulation, the presence of land-use change complicates the analysis of feedbacks.
1102 Land-use change is not a feedback process, yet owing to the C4MIP simulation design, carbon losses (or
1103 gains) due to land use change are confounded with the carbon-concentration feedback derived from a
1104 biogeochemically coupled scenario simulation. If we disregard agricultural areas, terrestrial carbon
1105 cycle feedback patterns in the spp534-over scenario are largely similar to those in the 1pctCO₂-cdr
1106 simulation, although some differences particularly in high northern latitudes due to the influences of
1107 non-CO₂ forcings exist.

1108 We conclude with some recommendations for future research and the design of future model
1109 intercomparison projects (MIPs) like C4MIP and CDRMIP. Identifying and better understanding the
1110 causes of differences in the lagged model response to decreasing emissions, which we have shown to
1111 increase the model disagreement under negative emissions should be pursued further with high
1112 priority. Both the integrated-flux (β and γ) and instantaneous-flux (B and Γ) based feedback metrics
1113 and their uncertainties become difficult to interpret in scenarios where atmospheric CO₂ concentration
1114 decreases, particularly in the extreme case when atmospheric CO₂ concentration and surface
1115 temperature approach their pre-industrial level. In the light of the discussion around CDR perhaps it is
1116 timely to rethink other but related forms of these metrics (e.g., see Chimuka et al. 2023) that describe
1117 the response of land and ocean carbon systems in scenarios of decreasing atmospheric CO₂ in a more
1118 robust manner.

1119 The 1pctCO₂ simulation combined with the 1pctCO₂-cdr simulation is an extremely idealized model
1120 experiment with huge (and infeasible) amounts of implied net-negative emissions and a discontinuity
1121 at year 140, where implied emissions jump from large positive to large negative values. As we know
1122 that carbon cycle feedbacks are scenario dependent, it would be preferable to assess these feedbacks
1123 using model simulations that have a more realistic emission pathway and that include more realistic
1124 amounts of net-negative emissions. Alternative idealized simulation designs that include negative
1125 emissions have been proposed in the literature (MacDougall 2019; Schwinger et al. 2022) and we have
1126 also considered the spp534-over scenario in this study. However, the presence of land-use change and
1127 variable non-CO₂ forcings in SSP scenarios complicates the quantification of carbon cycle feedbacks.
1128 Whether this problem can be solved for future phases of C4MIP by providing more detailed model
1129 output or by requesting additional idealized experiments (e.g., scenario simulations with fixed land use)
1130 should be discussed in the C4MIP community.

1131 Finally, most proposed negative emission options would be realized by manipulating the terrestrial or
1132 oceanic carbon sinks (e.g., bioenergy with carbon capture and storage, afforestation or ocean
1133 alkalization), thereby not only changing the atmospheric CO₂ concentration and possibly the surface
1134 climate but also the carbon cycle feedbacks themselves. Such interactions go beyond what can be
1135 addressed with the traditional C4MIP design of fully- and biogeochemically coupled ESM simulations.
1136 Consequently, a new framework for determining feedbacks caused by large scale CDR in realistic
1137 scenarios of CDR deployment is needed and should be developed in close collaboration with the
1138 integrated assessment modeling community that will create such scenarios.

Deleted: simulation. NorESM2 has the lowest transient climate response of the ESMs considered here and we therefore expect that other models might show an earlier and larger permafrost carbon release

Deleted: SSP5-3.4-OS

Deleted: SSP5-3.4-OS

Deleted: We expect that understanding and reducing the large uncertainties in the response of ESMs to changes in atmospheric CO₂ and surface climate, particularly during phases of negative emissions, remains a research topic of high relevance. Here, we have shown that the uncertainties (model disagreement) in feedback metrics increases during phases of negative emissions, and that this increase, for most of the feedback metrics, cannot be explained by a linear accumulation of uncertainty with progressing simulation time.

Deleted: such increased

Deleted: ¶

Deleted: were designed at a time when nearly all future climate change scenarios were characterized by continuously increasing atmospheric CO₂. Indeed both metrics perform well for such scenarios and have allowed us to compare the strength of carbon-concentration and carbon-climate feedbacks across models, albeit with

Deleted: well-known caveats (e.g., their scenario dependence). However,...

Deleted: , these metrics become difficult to interpret

Deleted: SSP5-3.4-OS

1167
1168
1169
1170

Data availability

1171 All CMIP6 model output data is freely available through the Earth System Grid Federation (for example,
1172 under <https://esgf-data.dkrz.de/search/cmip6-dkrz/>). The model output data of the 1pctCO₂-cdr-bgc
1173 simulation will be made publicly available upon final acceptance of this manuscript.

1174
1175

1176 **Competing interests**

1177 None of the authors has any competing interests.

1178
1179

1180 **Acknowledgements**

1181 A.A., J.S., and H.L. were supported by the Research council of Norway through the project IMPOSE
1182 (grant no. 294930). J.S. and H.L. also received funding from the European Union's Horizon Europe
1183 research and innovation programme (project RESCUE, grant agreement no. 101056939).
1184 Supercomputing and storage resources for additional NorESM2 simulations were provided by UNINETT
1185 Sigma2 (projects nn9708k/ns9708k). T.H. was supported by the Integrated Research Program for
1186 Advancing Climate Models (TOUGOU, grant number JPMXD0717935715) and the Program for the
1187 Advanced Studies of Climate Change Projection (SENTAN, grant number JPMXD0722681344) from the
1188 Ministry of Education, Culture, Sports, Science and Technology (MEXT), Japan. C.D.J. and S.L. were
1189 supported by the Joint UK BEIS/Defra Met Office Hadley Centre Climate Programme (GA01101), and
1190 the European Union's Horizon 2020 research and innovation programme under Grant Agreement No
1191 101003536 (ESM2025 - Earth System Models for the Future). R.S. and Y.S.-F. are grateful for the support
1192 of the team in charge of the CNRM-CM climate model. Supercomputing time was provided by the
1193 Meteo-France/DSI supercomputing center. R.S. acknowledges the European Union's Horizon 2020
1194 research and innovation program under grant agreement No. 101003536 (ESM2025 – Earth System
1195 Models for the Future). Y.S.-F. acknowledges the TRIATLAS project under the grant agreement No
1196 817578 and the COMFORT project under the grant agreement No 820989. [J.T. acknowledges the](#)
1197 [OceanICU project under the grant agreement no. 101083922.](#)

1198

1199 We acknowledge the World Climate Research Programme, which, through its Working Group on
1200 Coupled Modelling, coordinated and promoted CMIP6. We thank the climate modeling groups for
1201 producing and making available their model output, the Earth System Grid Federation (ESGF) for
1202 archiving the data and providing access, and the multiple funding agencies who support CMIP6 and
1203 ESGF.
1204

1205 The work reflects only the authors' view; the European Commission and their executive agency are
1206 not responsible for any use that may be made of the information the work contains.

1207
1208
1209

1210 References

- 1211 Armstrong McKay, D. I., and Coauthors, 2022: Exceeding 1.5°C global warming could trigger multiple
1212 climate tipping points. *Science*, **377**, eabn7950, <https://doi.org/10.1126/science.abn7950>.
- 1213 Arora, V. K., and Coauthors, 2013: Carbon–Concentration and Carbon–Climate Feedbacks in CMIP5
1214 Earth System Models. *J. Clim.*, **26**, 5289–5314, <https://doi.org/10.1175/JCLI-D-12-00494.1>.
- 1215 ———, and Coauthors, 2020: Carbon–concentration and carbon–climate feedbacks in CMIP6 models
1216 and their comparison to CMIP5 models. *Biogeosciences*, **17**, 4173–4222,
1217 <https://doi.org/10.5194/bg-17-4173-2020>.
- 1218 Bertini, L., and J. Tjiputra, 2022: Biogeochemical Timescales of Climate Change Onset and Recovery
1219 in the North Atlantic Interior Under Rapid Atmospheric CO₂ Forcing. *J. Geophys. Res. Oceans*,
1220 **127**, e2021JC017929, <https://doi.org/10.1029/2021JC017929>.
- 1221 Boer, G. J., and V. Arora, 2009: Temperature and concentration feedbacks in the carbon cycle.
1222 *Geophys. Res. Lett.*, **36**, <https://doi.org/10.1029/2008GL036220>.
- 1223 Boucher, O., and Coauthors, 2012: Reversibility in an Earth System model in response to CO₂
1224 concentration changes. *Environ. Res. Lett.*, **7**, 024013, [https://doi.org/10.1088/1748-](https://doi.org/10.1088/1748-9326/7/2/024013)
1225 [9326/7/2/024013](https://doi.org/10.1088/1748-9326/7/2/024013).
- 1226 Canadell, J. G., and Coauthors, 2021: Global carbon and other biogeochemical cycles and feedbacks.
1227 *Climate Change 2021: The Physical Science Basis. Contribution of Working Group I to the*
1228 *Sixth Assessment Report of the Intergovernmental Panel on Climate Change*, V. Masson-
1229 Delmotte et al., Eds., Cambridge University Press.
- 1230 [Chimuka, V. R., C. M. Nzotungicimpaye, and K. Zickfeld, 2023: Quantifying land carbon cycle](https://doi.org/10.5194/bg-20-2283-2023)
1231 [feedbacks under negative CO₂ emissions. *Biogeosciences*, **20**, 2283–2299,](https://doi.org/10.5194/bg-20-2283-2023)
1232 <https://doi.org/10.5194/bg-20-2283-2023>.
- 1233 Ciais, P., and Coauthors, 2013: Carbon and other biogeochemical cycles. *Climate Change 2013: The*
1234 *Physical Science Basis. Contribution of Working Group I to the Fifth Assessment Report of the*
1235 *Intergovernmental Panel on Climate Change*, Cambridge University Press, 465–570.
- 1236 Eyring, V., S. Bony, G. A. Meehl, C. A. Senior, B. Stevens, R. J. Stouffer, and K. E. Taylor, 2016:
1237 Overview of the Coupled Model Intercomparison Project Phase 6 (CMIP6) experimental design
1238 and organization. *Geosci. Model Dev.*, **9**, 1937–1958, [https://doi.org/10.5194/gmd-9-1937-](https://doi.org/10.5194/gmd-9-1937-2016)
1239 [2016](https://doi.org/10.5194/gmd-9-1937-2016).
- 1240 Feng, J., and Coauthors, 2020: Warming-induced permafrost thaw exacerbates tundra soil carbon
1241 decomposition mediated by microbial community. *Microbiome*, **8**, [3](https://doi.org/10.1186/s40168-019-0778-3),
1242 <https://doi.org/10.1186/s40168-019-0778-3>.
- 1243 [Forster, P. M., and Coauthors, 2023: Indicators of Global Climate Change 2022: annual update](https://doi.org/10.5194/essd-15-2295-2023)
1244 [of large-scale indicators of the state of the climate system and human influence. *Earth*](https://doi.org/10.5194/essd-15-2295-2023)
1245 [System Science Data](https://doi.org/10.5194/essd-15-2295-2023), **15**, 2295–2327, <https://doi.org/10.5194/essd-15-2295-2023>.
- 1246 Friedlingstein, P., J.-L. Dufresne, P. M. Cox, and P. Rayner, 2003: How positive is the feedback
1247 between climate change and the carbon cycle? *Tellus B Chem. Phys. Meteorol.*, **55**, 692–700,
1248 <https://doi.org/10.3402/tellusb.v55i2.16765>.
- 1249 ———, and Coauthors, 2006: Climate–Carbon Cycle Feedback Analysis: Results from the C4MIP
1250 Model Intercomparison. *J. Clim.*, **19**, 3337–3353, <https://doi.org/10.1175/JCLI3800.1>.
- 1251 Gasser, T., and Coauthors, 2018: Path-dependent reductions in CO₂ emission budgets caused by

Deleted: , 3, <https://doi.org/10.1186/s40168-019-0778-3>.

1253 permafrost carbon release. *Nat. Geosci.*, **11**, 830–835, [https://doi.org/10.1038/s41561-018-](https://doi.org/10.1038/s41561-018-0227-0)
1254 [0227-0](https://doi.org/10.1038/s41561-018-0227-0).

1255 Geden, O., and A. Lössel, 2017: Define limits for temperature overshoot targets. *Nat. Geosci.*, **10**,
1256 881–882, <https://doi.org/10.1038/s41561-017-0026-z>.

1257 Gillett, N. P., V. K. Arora, D. Matthews, and M. R. Allen, 2013: Constraining the Ratio of Global
1258 Warming to Cumulative [CO₂ Emissions Using CMIP5 Simulations](#). *J. Clim.*, **26**, 6844–6858,
1259 <https://doi.org/10.1175/JCLI-D-12-00476.1>.

1260 Goodwin, P., A. Katavouta, V. M. Roussenov, G. L. Foster, E. J. Rohling, and R. G. Williams, 2018:
1261 Pathways to 1.5 °C and 2 °C warming based on observational and geological constraints. *Nat.*
1262 *Geosci.*, **11**, 102–107, <https://doi.org/10.1038/s41561-017-0054-8>.

1263 Gregory, J. M., C. D. Jones, P. Cadule, and P. Friedlingstein, 2009: Quantifying Carbon Cycle
1264 Feedbacks. *J. Clim.*, **22**, 5232–5250, <https://doi.org/10.1175/2009JCLI2949.1>.

1265 Hajima, T., and Coauthors, 2020: Development of the MIROC-ES2L Earth system model and the
1266 evaluation of biogeochemical processes and feedbacks. *Geosci. Model Dev.*, **13**, 2197–2244,
1267 <https://doi.org/10.5194/gmd-13-2197-2020>.

1268 Hugelius, G., and Coauthors, 2014: Estimated stocks of circumpolar permafrost carbon with quantified
1269 uncertainty ranges and identified data gaps. *Biogeosciences*, **11**, 6573–6593,
1270 <https://doi.org/10.5194/bg-11-6573-2014>.

1271 Jeltsch-Thömmes, A., T. F. Stocker, and F. Joos, 2020: Hysteresis of the Earth system under positive
1272 and negative CO₂ emissions. *Environ. Res. Lett.*, **15**,
1273 124026, <https://doi.org/10.1088/1748-9326/abc4af>.

1274 Jones, C. D., and Coauthors, 2016a: Simulating the Earth system response to negative emissions.
1275 *Environ. Res. Lett.*, **11**, 095012, <https://doi.org/10.1088/1748-9326/11/9/095012>.

1276 Jones, C. D., and Coauthors, 2016b: C4MIP – The Coupled Climate–Carbon Cycle Model
1277 Intercomparison Project: experimental protocol for CMIP6. *Geosci. Model Dev.*, **9**, 2853–2880,
1278 <https://doi.org/10.5194/gmd-9-2853-2016>.

1279 Keller, D. P., and Coauthors, 2018: The Carbon Dioxide Removal Model Intercomparison Project
1280 (CDRMIP): rationale and experimental protocol for CMIP6. *Geosci. Model Dev.*, **11**, 1133–
1281 1160, <https://doi.org/10.5194/gmd-11-1133-2018>.

1282 [Krause, A., A. Arneeth, P. Anthoni, and A. Rammig, 2020: Legacy effects from historical
1283 environmental changes dominate future terrestrial carbon uptake, *Earth's Future*, **8**,
1284 \[e2020EF001674\]\(https://doi.org/10.1029/2020EF001674\), <https://doi.org/10.1029/2020EF001674>.](#)

1285 Lawrence, D. M., and Coauthors, 2019: The Community Land Model Version 5: Description of New
1286 Features, Benchmarking, and Impact of Forcing Uncertainty. *J. Adv. Model. Earth Syst.*, **11**,
1287 4245–4287, <https://doi.org/10.1029/2018MS001583>.

1288 Lenton, T. M., J. Rockström, O. Gaffney, S. Rahmstorf, K. Richardson, W. Steffen, and H. J.
1289 Schellnhuber, 2019: Climate tipping points — too risky to bet against. *Nature*, **575**, 592–595,
1290 <https://doi.org/10.1038/d41586-019-03595-0>.

1291 Li, X., K. Zickfeld, S. Mathesius, K. Kohfeld, and J. B. R. Matthews, 2020: Irreversibility of Marine
1292 Climate Change Impacts Under Carbon Dioxide Removal. *Geophys. Res. Lett.*, **47**,
1293 e2020GL088507, <https://doi.org/10.1029/2020GL088507>.

1294 Liang, Y.-C., L. M. Polvani, and I. Mitevski, 2022: Arctic amplification, and its seasonal migration,
1295 over a wide range of abrupt [CO₂ forcing](#). *Npj Clim. Atmospheric Sci.*, **5**, 14,
1296 <https://doi.org/10.1038/s41612-022-00228-8>.

1297 Liddicoat, S. K., and Coauthors, 2021: Compatible Fossil Fuel [CO₂ Emissions in the CMIP6 Earth
1298 System Models' Historical and Shared Socioeconomic Pathway Experiments of the Twenty-
1299 First Century](#). *J. Clim.*, **34**, 2853–2875, <https://doi.org/10.1175/JCLI-D-19-0991.1>.

1300 MacDougall, A. H., K. Zickfeld, R. Knutti, and H. D. Matthews, 2015: Sensitivity of carbon budgets to

Deleted: CO2 Emissions Using CMIP5 Simulations.

Deleted: Jenkins, M., and A. Dai, 2021: The Impact of Sea-Ice Loss on Arctic Climate Feedbacks and Their Role for Arctic Amplification. *Geophys. Res. Lett.*, **48**, <https://doi.org/10.1029/2021GL094599>.

Deleted: , <https://doi.org/10.5194/gmd-11-1133-2018>.

Deleted: CO2 forcing.

Deleted: CO2 Emissions in the CMIP6 Earth System Models' Historical and Shared Socioeconomic Pathway Experiments of the Twenty-First Century.

1311 permafrost carbon feedbacks and non-CO₂ forcings. *Environ. Res. Lett.*, **10**, 125003,
 1312 <https://doi.org/10.1088/1748-9326/10/12/125003>.

1313 Mathesius, S., M. Hofmann, K. Caldeira, and H. J. Schellnhuber, 2015: Long-term response of oceans
 1314 to CO₂ removal from the atmosphere. *Nat. Clim. Change*, **5**, 1107–1113,
 1315 <https://doi.org/10.1038/nclimate2729>.

1316 Meehl, G. A., C. A. Senior, V. Eyring, G. Flato, J.-F. Lamarque, R. J. Stouffer, K. E. Taylor, and M.
 1317 Schlund, 2020: Context for interpreting equilibrium climate sensitivity and transient climate
 1318 response from the CMIP6 Earth system models. *Sci. Adv.*, **6**, eaba1981,
 1319 <https://doi.org/10.1126/sciadv.aba1981>.

1320 Melnikova, I., and Coauthors, 2021: Carbon Cycle Response to Temperature Overshoot Beyond 2°C:
 1321 An Analysis of CMIP6 Models. *Earths Future*, **9**, e2020EF001967,
 1322 <https://doi.org/10.1029/2020EF001967>.

1323 Melnikova, I., and Coauthors, 2022: Impact of bioenergy crop expansion on climate–carbon cycle
 1324 feedbacks in overshoot scenarios. *Earth Syst. Dyn.*, **13**, 779–794, [https://doi.org/10.5194/esd-](https://doi.org/10.5194/esd-13-779-2022)
 1325 [13-779-2022](https://doi.org/10.5194/esd-13-779-2022).

1326 O’Neill, B. C., E. Kriegler, K. Riahi, K. L. Ebi, S. Hallegatte, T. R. Carter, R. Mathur, and D. P. van
 1327 Vuuren, 2014: A new scenario framework for climate change research: the concept of shared
 1328 socioeconomic pathways. *Clim. Change*, **122**, 387–400, [https://doi.org/10.1007/s10584-013-](https://doi.org/10.1007/s10584-013-0905-2)
 1329 [0905-2](https://doi.org/10.1007/s10584-013-0905-2).

1330 O’Neill, B. C., and Coauthors, 2016: The Scenario Model Intercomparison Project (ScenarioMIP) for
 1331 CMIP6. *Geosci. Model Dev.*, **9**, 3461–3482, <https://doi.org/10.5194/gmd-9-3461-2016>.

1332 Park, S.-W., and J.-S. Kug, 2022: A decline in atmospheric CO₂ levels under negative emissions may
 1333 enhance carbon retention in the terrestrial biosphere. *Commun. Earth Environ.*, **3**, 1–8,
 1334 <https://doi.org/10.1038/s43247-022-00621-4>.

1335 Rantanen, M., A.Y. Karpechko, A. Lipponen, K. Nordling, O. Hyvärinen, K. Ruosteenoja, T.
 1336 Vihma, and A. Laaksonen, 2022: The Arctic has warmed nearly four times faster than the globe
 1337 since 1979. *Commun Earth Environ.* **3**, 168. <https://doi.org/10.1038/s43247-022-00498-3>.

1338 Riahi, K., and Coauthors, 2021: Cost and attainability of meeting stringent climate targets without
 1339 overshoot. *Nat. Clim. Change*, **11**, 1063–1069, <https://doi.org/10.1038/s41558-021-01215-2>.

1340 Ricke, K. L., R. J. Millar, and D. G. MacMartin, 2017: Constraints on global temperature target
 1341 overshoot. *Sci. Rep.*, **7**, 14743, <https://doi.org/10.1038/s41598-017-14503-9>.

1342 Rogelj, J., M. Meinshausen, M. Schaeffer, R. Knutti, and K. Riahi, 2015: Impact of short-lived non-CO
 1343 CO_2 mitigation on carbon budgets for stabilizing global
 1344 warming. *Environ. Res. Lett.*, **10**, 075001, <https://doi.org/10.1088/1748-9326/10/7/075001>.

1345 Roy, T., and Coauthors, 2011: Regional Impacts of Climate Change and Atmospheric CO₂ on Future
 1346 Ocean Carbon Uptake: A Multimodel Linear Feedback Analysis. *J. Clim.*, **24**, 2300–2318,
 1347 <https://doi.org/10.1175/2010JCLI3787.1>.

1348 ———, J. B. Sallée, L. Bopp, and N. Metzl, 2021: Diagnosing CO₂-Emission-Induced Feedbacks
 1349 between the Southern Ocean Carbon Cycle and the Climate System: A Multiple Earth System
 1350 Model Analysis Using a Water Mass Tracking Approach. *J. Clim.*, **34**, 9071–9092,
 1351 <https://doi.org/10.1175/JCLI-D-20-0889.1>.

1352 Santana-Falcón, Y., and Coauthors, 2023: Irreversible loss in marine ecosystem habitability
 1353 after a temperature overshoot. *Commun Earth Environ* **4**, 343.
 1354 <https://doi.org/10.1038/s43247-023-01002-1>.

1355 Schimel, D., B. B. Stephens, and J. B. Fisher, 2015: Effect of increasing CO₂ on the terrestrial carbon
 1356 cycle. *Proc. Natl. Acad. Sci.*, **112**, 436–441, <https://doi.org/10.1073/pnas.1407302112>.

1357 Schuur, E. A. G., and Coauthors, 2015: Climate change and the permafrost carbon feedback. *Nature*,
 1358 **520**, 171–179, <https://doi.org/10.1038/nature14338>.

Deleted: CO2 levels under negative emissions may enhance carbon retention in the terrestrial biosphere.

Deleted: <https://doi.org/10.1038/s43247-022-00621-4>.

Deleted: CO2 on Future Ocean Carbon Uptake: A Multimodel Linear Feedback Analysis.

Deleted: CO2-Emission-Induced Feedbacks between the Southern Ocean Carbon Cycle and the Climate System: A Multiple Earth System Model Analysis Using a Water Mass Tracking Approach.

Deleted: <https://doi.org/10.1175/JCLI-D-20-0889.1>.

Deleted: CO2 on the terrestrial carbon cycle.

- 1370 Schwinger, J., and J. Tjiputra, 2018: Ocean Carbon Cycle Feedbacks Under Negative Emissions.
1371 *Geophys. Res. Lett.*, **45**, 5062–5070, <https://doi.org/10.1029/2018GL077790>.
- 1372 —, and Coauthors, 2014: Nonlinearity of Ocean Carbon Cycle Feedbacks in CMIP5 Earth System
1373 Models. *J. Clim.*, **27**, 3869–3888, <https://doi.org/10.1175/JCLI-D-13-00452.1>.
- 1374 —, A. Asaadi, N. J. Steinert, and H. Lee, 2022: Emit now, mitigate later? Earth system reversibility
1375 under overshoots of different magnitudes and durations. *Earth Syst. Dyn.*, **13**, 1641–1665,
1376 <https://doi.org/10.5194/esd-13-1641-2022>.
- 1377 Séférian, R., and Coauthors, 2019: Evaluation of CNRM Earth System Model, CNRM-ESM2-1: Role
1378 of Earth System Processes in Present-Day and Future Climate. *J. Adv. Model. Earth Syst.*, **11**,
1379 4182–4227, <https://doi.org/10.1029/2019MS001791>.
- 1380 Séférian, R., and Coauthors, 2020: Tracking Improvement in Simulated Marine
1381 Biogeochemistry Between CMIP5 and CMIP6. *Curr Clim Change Rep* 6, 95–119.
1382 <https://doi.org/10.1007/s40641-020-00160-0>.
- 1383 Seland, Ø., and Coauthors, 2020: Overview of the Norwegian Earth System Model (NorESM2) and
1384 key climate response of CMIP6 DECK, historical, and scenario simulations. *Geosci. Model*
1385 *Dev.*, **13**, 6165–6200, <https://doi.org/10.5194/gmd-13-6165-2020>.
- 1386 Sellar, A. A., and Coauthors, 2019: UKESM1: Description and Evaluation of the U.K. Earth System
1387 Model. *J. Adv. Model. Earth Syst.*, **11**, 4513–4558, <https://doi.org/10.1029/2019MS001739>.
- 1388 Smith, S. L., H. B. O'Neill, K. Isaksen, J. Noetzli, and V. E. Romanovsky, 2022: The changing thermal
1389 state of permafrost. *Nat. Rev. Earth Environ.*, **3**, 10–23, [https://doi.org/10.1038/s43017-021-](https://doi.org/10.1038/s43017-021-00240-1)
1390 [00240-1](https://doi.org/10.1038/s43017-021-00240-1).
- 1391 Smith, S. M., and Coauthors, 2023: The State of Carbon Dioxide Removal - 1st Edition. The
1392 State of Carbon Dioxide Removal. doi:10.17605/OSF.IO/W3B4Z.
- 1393 Swart, N. C., and Coauthors, 2019: The Canadian Earth System Model version 5 (CanESM5.0.3).
1394 *Geosci. Model Dev.*, **12**, 4823–4873, <https://doi.org/10.5194/gmd-12-4823-2019>.
- 1395 Taylor, K. E., R. J. Stouffer, and G. A. Meehl, 2012: An Overview of CMIP5 and the Experiment
1396 Design. *Bull. Am. Meteorol. Soc.*, **93**, 485–498, <https://doi.org/10.1175/BAMS-D-11-00094.1>.
- 1397 Tharammal, T., G. Bala, N. Devaraju, and R. Nemani, 2019: A review of the major drivers of the
1398 terrestrial carbon uptake: model-based assessments, consensus, and uncertainties. *Environ. Res.*
1399 *Lett.*, **14**, 093005, <https://doi.org/10.1088/1748-9326/ab3012>.
- 1400 Tjiputra, J. F., and Coauthors, 2020: Ocean biogeochemistry in the Norwegian Earth System Model
1401 version 2 (NorESM2). *Geosci. Model Dev.*, **13**, 2393–2431, [https://doi.org/10.5194/gmd-13-](https://doi.org/10.5194/gmd-13-2393-2020)
1402 [2393-2020](https://doi.org/10.5194/gmd-13-2393-2020).
- 1403 Tokarska, K. B., and K. Zickfeld, 2015: The effectiveness of net negative carbon dioxide emissions in
1404 reversing anthropogenic climate change. *Environ. Res. Lett.*, **10**, 094013,
1405 <https://doi.org/10.1088/1748-9326/10/9/094013>.
- 1406 V. Masson-Delmotte, P. Zhai, H.-O. Pörtner, D. Roberts, J. Skea, P.R. Shukla, A. Pirani, and W.
1407 Moufouma-Okia, C. Péan, R. Pidcock, S. Connors, J.B.R. Matthews, Y. Chen, X. Zhou, M.I.
1408 Gomis, E. Lonnoy, T. Maycock, M. Tignor, and T. Waterfield, 2018: IPCC, 2018: Summary for
1409 Policymakers. In: Global Warming of 1.5°C. An IPCC Special Report on the impacts of global
1410 warming of 1.5°C above pre-industrial levels and related global greenhouse gas emission
1411 pathways, in the context of strengthening the global response to the threat of climate change,
1412 sustainable development, and efforts to eradicate poverty, 32 pp. <https://www.ipcc.ch/sr15/>
1413 (Accessed June 21, 2021).
- 1414 de Vrese, P., and V. Brovkin, 2021: Timescales of the permafrost carbon cycle and legacy effects of
1415 temperature overshoot scenarios. *Nat. Commun.*, **12**, 2688, [https://doi.org/10.1038/s41467-021-](https://doi.org/10.1038/s41467-021-23010-5)
1416 [23010-5](https://doi.org/10.1038/s41467-021-23010-5).
- 1417 Wu, P., J. Ridley, A. Pardaens, R. Levine, and J. Lowe, 2015: The reversibility of CO₂ induced climate
1418 change. *Clim. Dyn.*, **45**, 745–754, <https://doi.org/10.1007/s00382-014-2302-6>.

Deleted: <https://doi.org/10.1029/2019MS001791>.

Deleted: <https://doi.org/10.1038/s43017-021-00240-1>.

Deleted: CO2 induced climate change.

- 1422 Yang, S., D. Tian, J. Chou, T. Wei, X. Zhu, and W. Dong, 2021: Reversibility of historical and future
1423 climate change with a complex earth system model. *Theor. Appl. Climatol.*, **146**, 1061–1068,
1424 <https://doi.org/10.1007/s00704-021-03757-z>.
- 1425 Yokohata, T., K. Saito, A. Ito, H. Ohno, K. Tanaka, T. Hajima, and G. Iwahana, 2020: Future
1426 projection of greenhouse gas emissions due to permafrost degradation using a simple numerical
1427 scheme with a global land surface model. *Prog. Earth Planet. Sci.*, **7**, 56,
1428 <https://doi.org/10.1186/s40645-020-00366-8>.
- 1429 Yoshikawa, C., M. Kawamiya, T. Kato, Y. Yamanaka, and T. Matsuno, 2008: Geographical
1430 distribution of the feedback between future climate change and the carbon cycle. *J. Geophys.*
1431 *Res. Biogeosciences*, **113**, <https://doi.org/10.1029/2007JG000570>.
- 1432
1433
1434
1435
1436
1437